https://doi.org/10.5194/egusphere-2025-6566
Preprint. Discussion started: 11 February 2026

Highlighting processes underlying the stability and hysteresis of the Antarctic Ice Sheet

Jan Swierczek-Jereczek[1,2], Jorge Alvarez-Solas[2], Alexander Robinson[3], Lucía Gutiérrez-González[1,2], and Marisa Montoya[1,2]

[1]Department Earth Physics and Astrophysics, Universidad Complutense de Madrid, Ciudad Universitaria, 28040, Madrid, Spain
[2]Geosciences Institute, CSIC-UCM, Calle Doctor Severo Ochoa, 7, 28040, Madrid, Spain
[3]Alfred Wegener Institute, Helmholtz Centre for Polar and Marine Research, Telegrafenberg A45, 14473, Potsdam, Germany

Correspondence: Jan Swierczek-Jereczek (janswier@ucm.es)

Abstract. Previous studies assessed that the Antarctic Ice Sheet (AIS) is subject to hysteresis, which means that if ice is lost due to an increase of temperature, a comparatively larger decrease is needed to recover the original state. This implies that the ice-sheet volume is multistable with respect to temperature and that ice loss can be abrupt and largely irreversible. This was simulated throughout a variety of modelling setups by using forcing ramps or steps which are prescribed offline. In contrast, the present study relies on an online, adaptive forcing technique in which the temperature anomalies are only increased when the rate of ice volume is below a tolerance that is significantly smaller than the present-day ice volume loss. Thus, previously unidentified bifurcations of the AIS are captured. We herein highlight the processes underlying such bifurcations. First, we show that the marine ice sheet instability (MISI) is an important driver of the numerous self-sustained retreats experienced by the East-Antarctic Subglacial Basins. Second, we highlight that the merger of two ice caps is an important driver of self-sustained regrowth. We refer to this as the perimeter feedback to generalise the interplay between ice-sheet geometry, ice flow, surface mass balance and thermodynamics which was partially described in studies considering the merger/collapse of ice saddles in different glaciological applications. We emphasise, for the first time to our knowledge, that the perimeter feedback applies beyond the case of a saddle merger/collapse and represents an important positive feedback on the mass balance of marine ice sheets, both at retreat and regrowth. Furthermore, by using a glacial isostatic adjustment (GIA) model of intermediate complexity, we highlight that, although GIA locally acts as a negative feedback on ice-sheet dynamics, it crucially eases other positive feedbacks on the continental scale and modulates the ice-ocean interaction. Finally, we show that the magnitude of the hysteresis might be larger than previously assessed in a similar modelling framework. We explain this by the increased sensitivity to the ocean of the present setup, which results from including a more marked nonlinearity of the basal friction law and an enhanced melt at the grounding zone due to tidal water intrusion, as suggested by recent publications.

1 Introduction

The Antarctic Ice Sheet (AIS) is expected to be the largest contributor to sea-level rise in the coming centuries due to anthropogenic warming (Fox-Kemper et al., 2021; Seroussi et al., 2020, 2024; Klose et al., 2024; Coulon et al., 2024, 2025).

https://doi.org/10.5194/egusphere-2025-6566
Preprint. Discussion started: 11 February 2026

Modelling studies furthermore indicate that the AIS displays a hysteresis behaviour, which means that if ice is lost due to an increase of global mean temperature (GMT), a comparatively larger decrease is needed to recover the original state (Huybrechts, 1994; Pollard and DeConto, 2005; Garbe et al., 2020; Van Breedam et al., 2023; Leloup et al., 2025). This implies that the AIS volume shows multistability with respect to global temperature and that future ice loss could be both abrupt, if a stable state disappears, and irreversible in practical terms, if the GMT decrease needed to recover the original configuration is infeasible. Understanding the future consequences of ice loss is not only a matter of how large but also how irreversible the committed sea-level rise will be. Characterising the hysteresis of the AIS is therefore key to inform mitigation and adaptation policies for coastal regions, which display some of the world's largest population densities (Kulp and Strauss, 2019). In addition, it can provide valuable insights on the past of the AIS, which was mostly exposed to warmer climates than present since its inception about $34\,\mathrm{Myr}$ ago (Hansen et al., 2013; Westerhold et al., 2020).

The mass balance of ice sheets is subject to positive and negative feedbacks, which promote the destabilisation and stabilisation of a given configuration, respectively. To date, the presence of an AIS hysteresis is explained in literature by highlighting three positive feedbacks. They are described below in the context of ice retreat but conversely apply to ice regrowth:

1. **Marine ice-sheet instability (MISI)**: when the grounding zone retreats on a retrograde bedrock, the ice thickness at the grounding zone increases. This significantly enhances the ice outflow at the grounding zone and leads to its further retreat until a prograde bedrock slope is reached again (Weertman, 1974; Schoof, 2007). This is considered the main driver of the self-sustained retreat of the West-Antarctic Ice Sheet (WAIS; Garbe et al., 2020; Leloup et al., 2025).

2. **Melt-elevation feedback**: when ice thins, its surface elevation is reduced, leaving it exposed to higher surface air temperatures due to the atmospheric lapse rate. This leads to more melt and further thinning. Huybrechts (1994) and Garbe et al. (2020) identified this mechanism as the main driver of mass loss of the East-Antarctic Ice Sheet (EAIS).

3. **Melt-albedo feedback**: when snow melts, bare ice is exposed and melt ponds can form. Furthermore, when ice retreats, bare rock and ocean are exposed, leading to a decreased albedo and an increased absorption of shortwave radiation. This in turn leads to higher global temperatures and an increased local amplification of the warming, which ultimately causes more melt and further decreases the albedo. Pollard and DeConto (2005); Van Breedam et al. (2023); Leloup et al. (2025) include this effect with various degrees of complexity and highlight it as the main driver of the self-sustained retreat of the EAIS for high warming.

Whereas some positive feedbacks are too weak to have a significant impact on the AIS hysteresis (e.g. creep instability, Clarke et al., 1977; Garbe et al., 2020), others are considered too speculative to be included in the present framework (marine ice-cliff instability, Pollard et al., 2015; Morlighem et al., 2024; Lipscomb et al., 2025). It is worth mentioning that glacial isostatic adjustment (GIA) provides a negative feedback on the melt-elevation and on MISI via the bedrock rebound following ice thinning. In the case of MISI, this is further reinforced by the local reduction in sea-surface elevation that results from the decreased gravitational pull after ice thinning (c.f. Gomez et al., 2012; Whitehouse et al., 2019, for a more detailed description of these effects).

https://doi.org/10.5194/egusphere-2025-6566
Preprint. Discussion started: 11 February 2026

In the aforementioned studies, the hysteresis diagram is either obtained by running step or ramp experiments. In the first case, the resolution of the forcing space is typically quite low: about ten equilibrium points cover either (1) $f_a = [0, 20]\,\mathrm{K}$, with f_a the regional atmospheric temperature anomaly (Huybrechts, 1994; Garbe et al., 2020) or (2) $[0.8, 8] \times \mathrm{piCO_2}$, with $\mathrm{piCO_2}$ the pre-industrial $\mathrm{CO_2}$ concentration (Leloup et al., 2025). This is problematic since a potential self-sustained retreat (or regrowth) happening between these points would be largely hidden. In the second case, using a ramp with very small rate of change partially addresses this problem, since it allows for a continuous sampling of the forcing space (Pollard and DeConto, 2005; Garbe et al., 2020; Van Breedam et al., 2023). However, the continuous increase of the forcing leads any self-sustained retreat (significant volume loss at constant forcing) to be misrepresented as a large sensitivity (significant volume loss over a small forcing increment). These caveats can be largely attributed to the fact that the step and ramp forcing are determined offline, i.e. without taking into consideration the current state of the ice sheet. This can however be addressed by computing the forcing online, based on the current rate of volume change. Along this line, we introduce a novel, online forcing technique in Sec. 2. We show that, although the results described in Sec. 3 are quantitatively similar to previous AIS hysteresis studies, they also display some qualitative differences, suggesting that some important feedbacks have been underestimated or even overlooked in previous studies. In Sec. 4, we discuss the limitations and implications of the obtained results before drawing some conclusions in Section 5.

2 Methods

2.1 Model setup

The simulations presented here are performed with Yelmo, a thermo-mechanically coupled 3D ice-sheet model (Robinson et al., 2020) that is interactively coupled to FastIsostasy, a 2D GIA model that accounts for the lateral variability of the solid-Earth structure and for the spatially heterogeneous sea-surface elevation resulting from gravitational anomalies (Swierczek-Jereczek et al., 2024). The lithospheric thickness and upper-mantle viscosity both vary laterally, with ranges of $20 - 300\,\mathrm{km}$ and $6 \cdot 10^{19} - 1.5 \cdot 10^{22}\,\mathrm{Pa\,s}$, respectively (Hazzard and Richards, 2024). The barystatic sea level evolves according to the AIS volume contributions, as described in Goelzer et al. (2020). The simulations are performed on a regular grid covering Antarctica with a horizontal resolution of $\Delta x = \Delta y = 16\,\mathrm{km}$ and, in the case of Yelmo, a vertical resolution of 10 quadratically scaled layers which range from $\Delta z \simeq 0.01 \cdot H$ at the base up to $\Delta z \simeq 0.4 \cdot H$ at the top. This is defined as a fraction of the ice thickness, H, due to the sigma-transform applied to the vertical dimension. The ice dynamics follows a Glen flow law with exponent $n = 3$ and enhancement factors of 1, 1 and 0.7 for the shear, stream and shelf regions, respectively. The velocity field is computed by using the depth-integrated viscosity approximation (DIVA; Goldberg, 2011; Robinson et al., 2022). Calving is parametrized through the von Mises criterion (Lipscomb et al., 2019). We use a partial melt parametrisation with tides (PMPT) at the grounding zone. This modification of Leguy et al. (2021) aims to represent the effect of tidal water intrusions that were recently observed in various regions of the AIS (Christianson et al., 2016; Chen et al., 2023; Rignot et al., 2024, respectively in Ross, Amery and Thwaites). PMPT applies a basal melt, $\dot{b}$, following:

https://doi.org/10.5194/egusphere-2025-6566
Preprint. Discussion started: 11 February 2026

$$\dot{b} = \begin{cases} \dot{b}_g & \text{if } H_{\mathrm{af}} \geq H_{\mathrm{t}}, \\ \dot{b}_f & \text{if } H_{\mathrm{af}} \leq 0, \\ w_g \cdot \dot{b}_g + w_f \cdot \dot{b}_f & \text{if } 0 < H_{\mathrm{af}} < H_{\mathrm{t}}. \end{cases} \tag{1}$$

Here, $\dot{b}_g$ represents the basal mass balance (BMB) of a fully grounded point, $\dot{b}_f$ the BMB of a fully floating point, and w_g, w_f are weighting factors that sum to 1. They account for the fact that the BMB at the grounding zone points is a mixture of $\dot{b}_g$ and $\dot{b}_f$, determined by the grounded fraction, $w_g = \min(H_{\mathrm{af}} \cdot H_{\mathrm{t}}^{-1}, 1)$, that accounts for tidal intrusion. By setting the tidal intrusion above flotation to $H_{\mathrm{t}} = 50\,\mathrm{m}$, the region where partial melt is applied reaches from a hundred metres up to a few kilometres upstream from the grounding line, depending on the gradient of ice thickness above flotation but limited by the horizontal grid resolution of $16\,\mathrm{km}$. Thus, we obtain a sub-grid behaviour that is very similar to observations (Fig. A1, Chen et al., 2023; Rignot et al., 2024) while reducing the parameterisation complexity compared to more comprehensive approaches (Robel et al., 2022; Ross et al., 2024). We emphasise that H_t represents the maximal ice thickness above flotation where tidal water can penetrate and not the anomaly of sea-surface elevation caused by tides, which is of a few metres at most (Chen et al., 2023; Rignot et al., 2024). Although a more comprehensive treatment of the water intrusion would require the inclusion of the bathymetry and ice flow (Ross et al., 2024), this is somewhat reflected by using the height above flotation to compute PMPT. Finally, the basal friction, $\boldsymbol{\tau}_b$, depends on the basal velocity, $\boldsymbol{u}_b$, following a regularized Coulomb friction law:

$$\boldsymbol{\tau}_b = N\, c_{b,\mathrm{ref}} \left(\frac{\boldsymbol{u}_b}{||\boldsymbol{u}_b|| + u_0} \right)^q . \tag{2}$$

The effective pressure, N, depends on the basal hydrology, which follows a local energy balance and a fixed till drainage rate (Bueler and van Pelt, 2015). The regularisation term, $u_0 = 100\,\mathrm{m\,s^{-1}}$, and the exponent governing the nonlinearity, $q = 0.2$, are fixed to values inferred from laboratory experiments for soft beds (Zoet and Iverson, 2020). The basal friction coefficient $c_{b,\mathrm{ref}}$ is inferred by inversion of the present-day ice thickness and ice velocity. This results in a modelled present-day state that is close to observations, in particular in terms of grounding-zone position (Fig. A2). The root mean square error in surface elevation and velocity yield $114\,\mathrm{m}$ and $96\,\mathrm{m\,yr^{-1}}$, respectively. Both of these values are well within the range of ISMIP6 models (Seroussi et al., 2020, 2024) and the grounding-zone position is close to the observed present-day one (Fig. 1).

The present setup does not include an energy balance model, and thereby lacks the representation of the melt-albedo feedback. This prevents from obtaining a realistic hysteresis of the AIS at high temperature anomalies but highlights the importance of other processes, which can be hidden by the dominant melt-albedo feedback (e.g. Leloup et al., 2025) in spite of their potential role in triggering it.

2.2 Forcing setup

To force the AIS, we impose a GMT anomaly with respect to pre-industrial climate (1850-1900), beginning at $f = 1.2\,\mathrm{K}$ to capture the GMT anomaly at year 2020. The GMT anomaly is converted into a regional atmospheric temperature anomaly,

https://doi.org/10.5194/egusphere-2025-6566
Preprint. Discussion started: 11 February 2026

$f_a = 1.8 \cdot f$, by using a fixed factor that was assessed for Antarctica in the polar amplification model inter-comparison project (Smith et al., 2019). This anomaly is uniformly added to the surface air temperature field of the latest present-day climatology produced by RACMO2.3 (Van Wessem et al., 2023). As the ice topography changes over time, the surface air temperature is modified according to a lapse rate of $-6.5\,\mathrm{K\,km^{-1}}$. The precipitation anomaly is computed through a fixed $5\%\,\mathrm{K^{-1}}$ factor (accounting for regional warming and elevation changes), and the surface melt is calculated with the positive degree day method (Reeh, 1989). In an ensemble of long-term CMIP5 and CMIP6 simulations, the warming of the Southern Ocean was assessed to be about 25% of the regional atmospheric one (Golledge et al., 2015). We therefore compute the regional oceanic temperature anomaly as $f_o = 0.25 \cdot 1.8 \cdot f$. This anomaly is uniformly added to the present-day ocean temperature field provided in Jourdain et al. (2020) and is subsequently converted into sub-shelf melting via the quadratic non-local law of Favier et al. (2019).

Table 1. Summary of the experiment names, their setup and the associated supplementary material that visualises the equilibrium evolution of the AIS. We strongly recommend watching the provided videos, which help to understand the results in a much more intuitive way.

Name	Description	Supplementary material
REF	Temperature anomalies applied to ocean and atmosphere GIA on	Video 1 (retreat); Video 5 (regrowth); Video 5b (regrowth, second part)
EQL	Equilibrium runs branched off from REF, same set-up	-
ATM	Temperature anomalies applied to atmosphere only ($f_o = 0$) GIA on	Video 2 (retreat); Video 6 (regrowth)
OCN	Temperature anomalies applied to ocean only ($f_a = 0$) GIA on	Video 3 (retreat)
UPL	Temperature anomalies applied to ocean and atmosphere GIA off: uplifted bed in equilibrium with ice-free Antarctica	Video 7 (regrowth)
DPR	Temperature anomalies applied to ocean and atmosphere GIA off: depressed bed in equilibrium with present-day AIS	Video 4 (retreat); Video 8 (regrowth)
HOW	Higher ocean warming than in REF ($f_o = 0.39 \cdot 1.8 \cdot f$) GIA on	-

To obtain the equilibrium diagram of the AIS, we introduce the adaptive quasi-equilibrium forcing (AQEF). This consists in ramping up the atmospheric and oceanic temperature anomalies with $\dot{f}_a = 1 \cdot 10^{-4}\,\mathrm{K\,yr^{-1}}$ and $\dot{f}_o = 0.25 \cdot 10^{-4}\,\mathrm{K\,yr^{-1}}$ when the change in ice mass, averaged over the last 100 years, is less than a threshold set to $\varepsilon = 40\,\mathrm{Gt\,yr^{-1}}$. The mass loss of Antarctica as inferred by altimetry, gravimetry and input-output method from 2008 to 2018 averaged about $150\,\mathrm{Gt\,yr^{-1}}$ (The IMBIE team, 2018), which is 3.75 times more than the threshold used here. If the aforementioned condition is not met, the forcing is maintained at its current level ($\dot{f}_a = \dot{f}_o = 0\,\mathrm{K\,yr^{-1}}$), which captures self-sustained ice loss more accurately than offline forcing techniques. For the cooling part of the experiment, we decrease the anomalies with $\dot{f}_a = 0.5 \cdot 10^{-4}\,\mathrm{K\,yr^{-1}}$, $\dot{f}_o = 0.125 \cdot 10^{-4}\,\mathrm{K\,yr^{-1}}$ and $\varepsilon = 20\,\mathrm{Gt\,yr^{-1}}$ to better capture the comparatively slow time scales of the regrowth process. The

https://doi.org/10.5194/egusphere-2025-6566
Preprint. Discussion started: 11 February 2026

combination of retreat and regrowth branches constitutes our reference transient experiment, further referred to as REF. To make sure that equilibrium is reached, a simulation is branched off from REF at about each 0.1 K of GMT anomaly and the forcing is subsequently maintained constant for 30 kyr (retreat) or 50 kyr (regrowth). The resulting set of equilibrium points constitutes the most reliable estimate of the AIS equilibrium provided here; we refer to this set of experiments as EQL. In the following subsections, we first study the retreat, then the regrowth and finally the hysteresis of the AIS, including a comparison to previous studies when possible. To highlight important processes, permutations of REF are performed throughout Sec. 3, as summarised in Table 1.

3 Results

3.1 Retreat branch

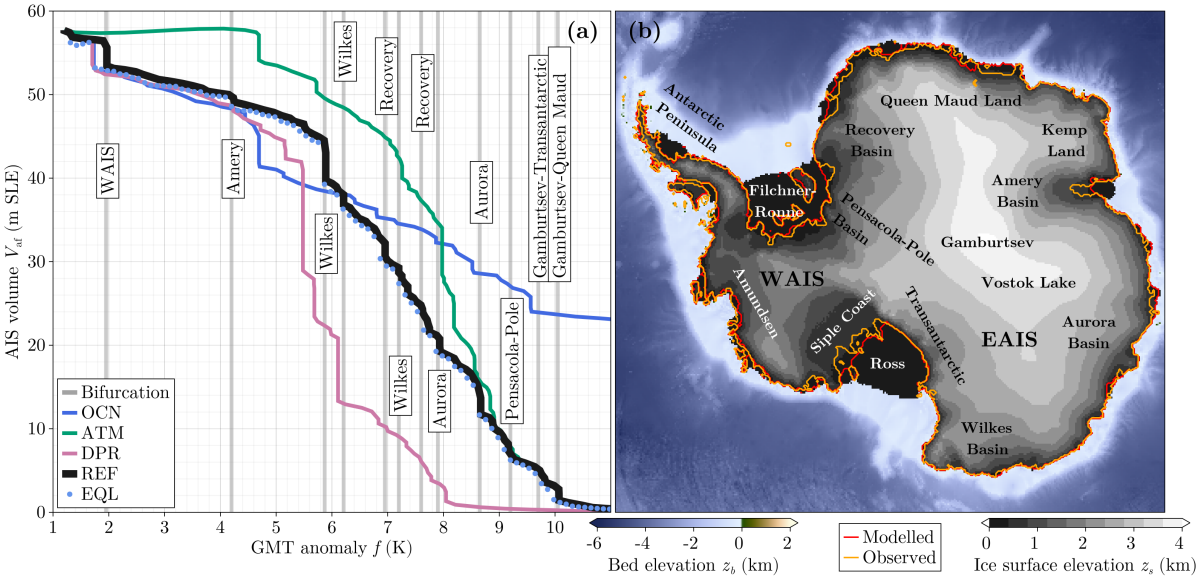

Figure 1. (a) Retreat branch of the AIS hysteresis (black), marked by self-sustained retreats highlighted by vertical shadings. The coloured curves show the equilibrium retreat when oceanic warming, atmospheric warming and GIA are deactivated, respectively (ATM, OCN and DPR). Here again, the retreat is marked by bifurcations, which are however not highlighted by vertical shadings for the clarity of the visualisation. (b) Modelled present-day state of the AIS, including the region names that are relevant for the description of the results.

3.1.1 Quasi-equilibrium as proxy for the equilibrium

The first striking behaviour observed in the equilibrium diagram of the AIS retreat is the close match between REF and EQL (Fig. 1.a). Thus, the AQEF results closely follow the true equilibrium, with a tendency to slightly overestimate the volume (on

https://doi.org/10.5194/egusphere-2025-6566
Preprint. Discussion started: 11 February 2026

average by $0.8\,\mathrm{mSLE}$). REF is hereafter used as a proxy for EQL, because it advantageously provides a continuous resolution of the AIS variables over the forcing values, which facilitates the disentanglement of processes. We stress that carrying out a single AQEF run is computationally cheaper than performing a large ensemble of equilibrium runs. Thus, AQEF represents a novel forcing technique that can be used in Earth-System model components to accurately approximate the equilibrium behaviour at low computational cost and almost no implementation effort.

3.1.2 Sensitivity and tipping behaviour

The AIS sensitivity to warming can be classified into three distinct phases. First, REF displays a phase of relatively small sensitivity to warming from $f = 1.2\,\mathrm{K}$ (global warming at year 2020 with respect to the 1850-1900 average) until $f = 5.9\,\mathrm{K}$. The volume loss over this span is of about 13 metres of sea-level equivalent (mSLE, Fig. 1.a), yielding an average ice loss per forcing degree of about $2.2\,\mathrm{mSLE\,K^{-1}}$. Subsequently, the sensitivity increases considerably until about $f = 9.2\,\mathrm{K}$, yielding an average value of $11.5\,\mathrm{mSLE\,K^{-1}}$. From there on, there is barely any ice left and the sensitivity converges to 0.

Furthermore, REF is punctuated by 12 self-sustained retreats (Fig. 1), also known as bifurcations or tipping points. They are characterised by an abrupt reduction of the ice volume at constant forcing (Armstrong McKay et al., 2022), as highlighted by the vertical shadings (Fig. 1.a). Here, we only highlight bifurcations that imply a volume loss of more than $0.5\,\mathrm{mSLE}$ and identify their associated regions based on Video 1 of the supplementary material. The existence of various bifurcations within the same system is known as fragmented tipping (Bastiaansen et al., 2022), which challenges the widespread understanding of tipping as being characterised by a single threshold. For instance, based on Garbe et al. (2020), Armstrong McKay et al. (2022) suggest a single tipping point of the East-Antarctic Subglacial Basins (EASBs). This is refuted by the current results, which show nine different bifurcation points for the EASBs. We however note that the exact amount of bifurcation points would likely be altered when including the melt-albedo feedback.

Among these bifurcation points, the retreat of the Wilkes Subglacial Basin (WSB) at $f = 5.9\,\mathrm{K}$ should be particularly highlighted, since it initiates the phase of increased sensitivity mentioned above. As shown in Fig. 2, the WSB retreat leads to a much lower surface elevation along the AIS margin in this region. This leads to a greatly reduced SMB as a consequence of the melt-elevation feedback which, prior to this, was largely inactive in the EAIS due to the absence of any significant retreat.

3.1.3 Driver of self-sustained retreats

As shown in Fig. 2 and particularly in Video 1 of the supplementary material, most self-sustained retreats occur in marine-based regions while being preceded by a localised acceleration of the ice flow, which leads to a substantial ice thinning and ungrounding. We investigate the drivers of these retreats in greater detail for the four largest bifurcations, highlighted in Fig. 2 and leading to sea-level contributions of about $3.5\,\mathrm{mSLE}$ (WAIS), $6\,\mathrm{mSLE}$ (WSB), $2\,\mathrm{mSLE}$ (Recovery Subglacial Basin, RSB), and $4\,\mathrm{mSLE}$ (Aurora Subglacial Basin, ASB), respectively.

To this end, we perform transects along the main direction of grounding-zone retreat, showing that all four bifurcations take place on marine-based sectors of the AIS with a retrograde bedrock below sea level. While the grounding zone slowly retreats over pinning points and prograde bedrock regions, it abruptly retreats over retrograde ones (Fig. 3, middle and right columns).

https://doi.org/10.5194/egusphere-2025-6566
Preprint. Discussion started: 11 February 2026

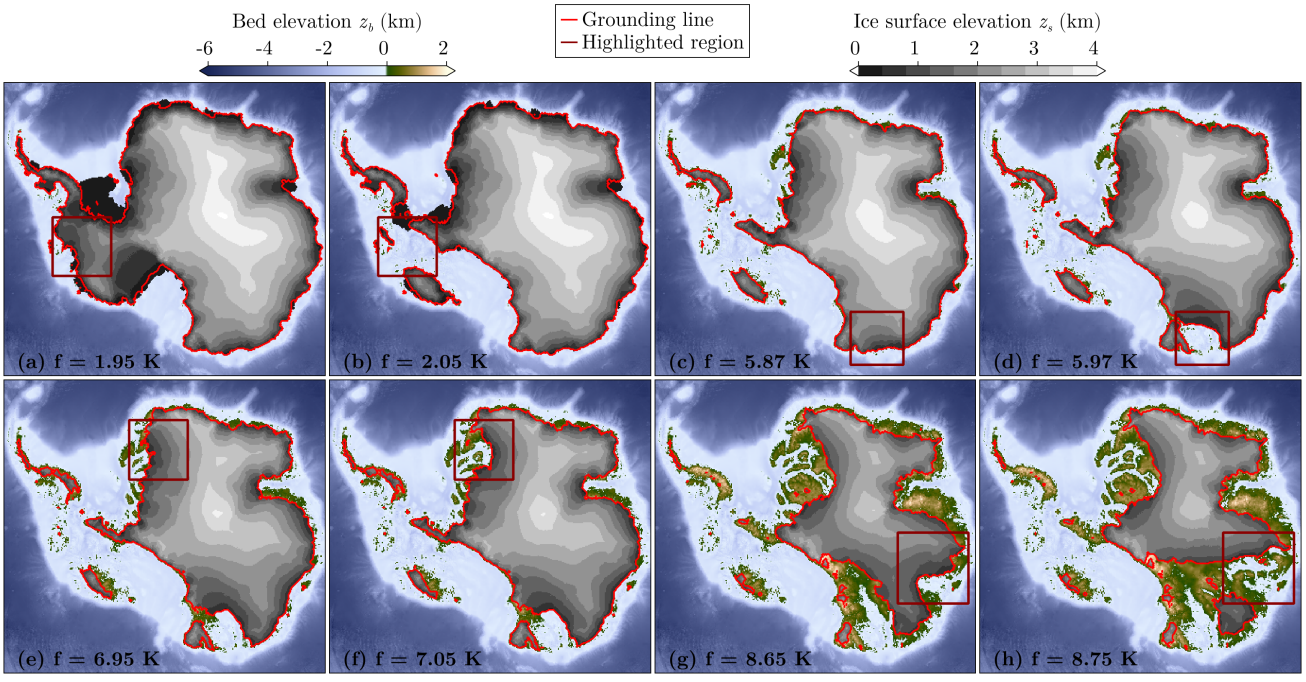

Figure 2. AIS states before and after the four largest bifurcation points of REF highlighted in Figure 1 for (a-b) the WAIS, (c-d) the Wilkes, (e-f) the Recovery and (g-h) the Aurora Subglacial Basins. The regions highlighted by the square frames help identify where the retreat occurs at each bifurcation.

As shown in Video 1 of the supplements, this ungrounding results in the formation of large ice shelves. Thus, the surface in contact with the ocean is largely increased, leading to an increased basal melt. This is observed in the time series of the regionally averaged BMB and is often accompanied by a decrease in surface mass balance (SMB) due to the melt-elevation feedback (Fig. 3, left column). Overall, this behaviour is characteristic of MISI.

Among the 12 bifurcation points identified, two of them occur in the EAIS interior and are therefore not driven by MISI. The first of them, at $f = 9.2\,\mathrm{K}$, is driven by the saddle collapse between the Gamburstev and the Transantarctic Mountains. The second, at $f = 10.1\,\mathrm{K}$, is driven by the saddle collapse between the Gamburstev and the Queen Maud Mountains (Fig. D2). A saddle collapse denotes the dissociation of the ice sheet into two distinct parts, which takes place at the saddle point between two domes and leads to a self-sustained, accelerated ice loss. This mechanism was already suggested to explain rapid retreats of the Laurentide Ice Sheet and invoked as a potential source of rapid sea-level rise and ocean freshening during deglaciation (Gregoire et al., 2012, 2016; Gomez et al., 2015; Matero et al., 2017, 2020; Lochte et al., 2019; Gauthier et al., 2020; Reyes et al., 2024), but was so far absent from the literature on the AIS stability. The physics underlying such an event is described with greater detail in Sec. 3.2 for the regrowth experiment, where it plays a much more important role.

https://doi.org/10.5194/egusphere-2025-6566
Preprint. Discussion started: 11 February 2026

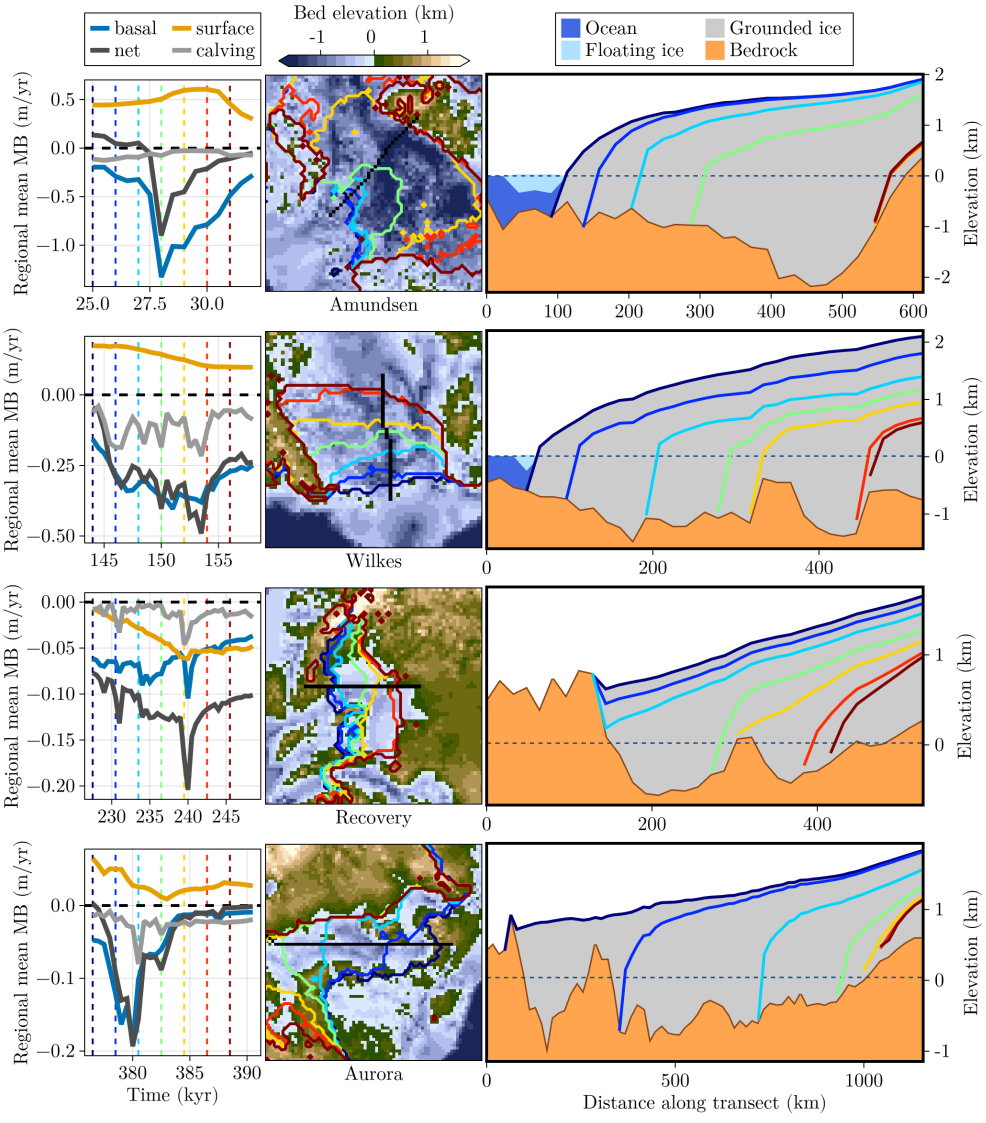

Figure 3. (Left column) Time series of the regionally-averaged mass balance (MB) terms; (Middle column) (x, y)-visualisation of the four regions highlighted in Fig. 2, including a transect (black) across the main direction of grounding-zone retreat; (Right column) ice-surface transect visualised in the (r, z) plane, with r the coordinate along the transect. The vertical lines in the MB time series are evenly spaced in time and correspond to the grounding-zone positions shown in (x, y) and to the ice profiles shown in (r, z).

https://doi.org/10.5194/egusphere-2025-6566
Preprint. Discussion started: 11 February 2026

3.1.4 Disentangling the role of oceanic and atmospheric forcing

To disentangle the contributions of the atmospheric and oceanic forcing, we perform two retreat runs, ATM and OCN, where only the atmospheric or the oceanic temperature anomalies are applied, respectively. Remarkably, OCN and REF largely coincide for $f \in [1.2, 4.4]\,\mathrm{K}$, whereas ATM and REF largely coincide for $f \in [8.6, 11]\,\mathrm{K}$ (Fig. 1.a). This indicates that the contribution of the oceanic forcing dominates in the first part of the diagram while the atmospheric forcing dominates in the last one, and both contribute significantly for $f \in [4.4, 8.6]\,\mathrm{K}$. Furthermore, OCN shows self-sustained grounding-zone retreats of the WAIS and WSB at $f = 1.7\,\mathrm{K}$ and $f = 4.7\,\mathrm{K}$, respectively. They are quantitatively similar to REF but take place for lower warming levels because the absence of atmospheric warming prevents the increase of SMB, thus facilitating earlier grounding-zone retreats. This is confirmed by the volume increase displayed by ATM for $f \in [1.2, 4.7]\,\mathrm{K}$. For $f > 4.7\,\mathrm{K}$, surface melt starts prevailing over accumulation and the atmospheric forcing transitions from being an inhibitor to being a facilitator of grounding-zone retreat. This explains why, beyond this point, the MISI-driven retreats of OCN are of smaller amplitude compared to REF, where MISI is greatly reinforced by surface melt. As shown in Video 3 of the supplementary material, OCN presents an AIS that is largely disconnected from the ocean for $f > 9.6\,\mathrm{K}$. This prevents any further melting and leads the retreat curve to flatten.

In ATM, many bifurcations are observed and correspond to self-sustained retreats over marine-based regions, preceded by an acceleration of the ice flow, as shown in Video 2 of the supplementary material. We therefore identify them as MISI events that are triggered by atmospheric warming at present-day ocean temperatures. The fact that atmospheric warming can lead to ice thinning at the grounding zone and thus trigger MISI is nothing that challenges the common understanding of ice-sheet modelling but was never pointed out to our knowledge.

3.1.5 On the role of GIA

To complement this perspective, we further perform a run where GIA is deactivated. Thus, the bathymetry is kept constant in the depressed state that is in equilibrium with the present-day AIS configuration. This experiment is therefore labelled as DPR and displays bifurcation points at lower warming levels and with larger amplitudes than in REF. For instance, the WAIS collapses at $f = 1.7\,\mathrm{K}$, with a sea-level contribution of about $4\,\mathrm{mSLE}$, whereas the WSB collapses at $f = 5.5$ with a contribution of $13\,\mathrm{mSLE}$ (Fig. 1. a). The lowering of the bifurcation point is due to the lack of GIA feedbacks before reaching a retrograde bed slope, whereas the increased magnitude of the bifurcation is due to the lack of GIA feedbacks during MISI, which leads to a much larger propagation of the instability throughout an oceanic basin, as shown in Video 4 of the supplementary material. Thus, whereas the WSB, RSB and ASB collapse in two distinct steps in REF, they each collapse in a single one in DPR. This reduces the fragmented nature of the AIS retreat. The largest difference between REF and DPR is observed at $V = 15\,\mathrm{mSLE}$, where it yields $\Delta f = 2.5\,\mathrm{K}$, and at $f = 6.1\mathrm{K}$, where it yields $\Delta V = 25\,\mathrm{mSLE}$. Thus, the GIA response shifts the AIS retreat to significantly higher warming levels, highlighting its role as an important negative feedback.

https://doi.org/10.5194/egusphere-2025-6566
Preprint. Discussion started: 11 February 2026

3.1.6 Conclusions on the equilibrium AIS retreat

In summary, the equilibrium behaviour of the AIS retreat, marked by more bifurcations than previously assumed, can be well resolved by the AQEF. Its sensitivity is mostly controlled by the ocean for small GMT increases, by the atmosphere for large GMT increases, and by a combination of both for intermediate values. Atmospheric warming acts as an inhibitor of mass loss at low temperature anomalies due to increased precipitation, and as facilitator at high temperature anomalies due to increased surface melting. The melt-elevation feedback therefore provides a strong control on the sensitivity of the AIS retreat but never represents the sole driver of a bifurcation. In contrast, MISI is the driver of most self-sustained retreats but only marginally affects the overall sensitivity via its interaction with the melt-elevation feedback. Remarkably, the low sensitivity regime that characterises the near future is challenging in terms of policy making: prior to their collapse, the WAIS and WSB show almost no sea-level contribution. In other words, no significant sea-level rise is simulated until a large, self-sustained one occurs.

3.2 Regrowth branch

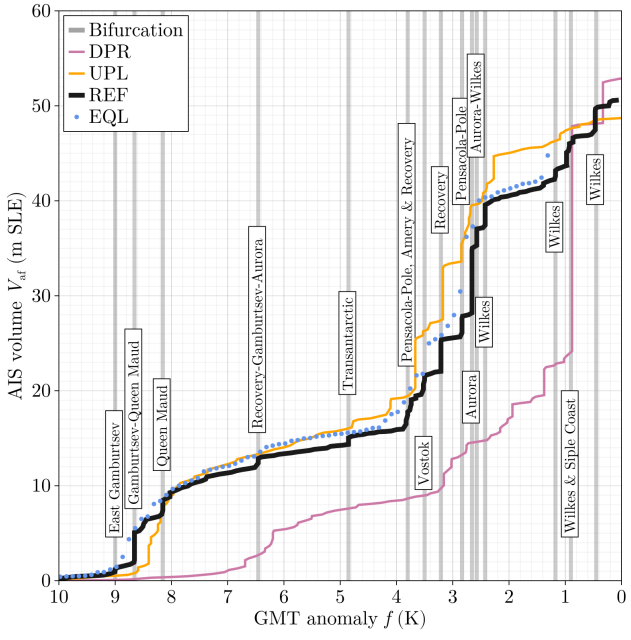

Figure 4. Regrowth branch of the AIS hysteresis (black), marked by self-sustained retreats highlighted by vertical shadings. The coloured curves show the equilibrium retreat when oceanic warming is deactivated (ATM), bedrock is kept constant at its present-day configuration (DPR) or in a fully uplifted configuration (UPL). Here again, the retreat is marked by bifurcations, which are however not highlighted by vertical shadings for the clarity of the visualisation.

https://doi.org/10.5194/egusphere-2025-6566
Preprint. Discussion started: 11 February 2026

3.2.1 Sensitivity and tipping behaviour

Similar to its retreat, the AIS regrowth shows a close match between REF and EQL, in spite of being marginally larger than at retreat ($1.2\,\mathrm{mSLE}$ on average) due to the long time scales associated with the regrowth. Here again, this motivates the use of REF as a proxy for EQL with continuous forcing values (Fig. 4). Glacial inception of the AIS begins around $f = 9\,\mathrm{K}$ in the Gamburtsev Mountains due to the low surface air temperatures resulting from the high elevation and the proximity to the South Pole. After this, the volume gain experiences four distinct phases of sensitivity (Fig. 4):

1. $9 \rightarrow 8\,\mathrm{K}$: Many isolated glaciers form in the East-Antarctic mountains. Their merger leads to a few self-sustained advances of the ice sheet (Fig. 5 and Video 5 of the supplementary material), driving a large volume increase from 1 to $10\,\mathrm{mSLE}$. This results in a large sensitivity of about $9\,\mathrm{mSLE\,K^{-1}}$ (Fig. 4).

2. $8 \rightarrow 3.8\,\mathrm{K}$: The EAIS advances until the coast, thus largely increasing its surface area (Fig. 5.d-f). However, the AIS remains relatively thin and the associated volume increase yields only about $8\,\mathrm{mSLE}$, leading to a sensitivity as little as $2\,\mathrm{mSLE\,K^{-1}}$ (Fig. 4). This phase is marked by comparatively few self-sustained advances which also result from merging various parts of the AIS (Video 5 of the supplementary material).

3. $3.8 \rightarrow 2.4\,\mathrm{K}$: The ocean has cooled sufficiently for the AIS to grow over marine regions. This happens in a self-sustained way in the EASBs, driving 7 distinct bifurcations. This leads to a large volume increase and a mean sensitivity of about $17.2\,\mathrm{mSLE\,K^{-1}}$.

4. $2.4 \rightarrow 0\,\mathrm{K}$: the EAIS has almost reached its present-day configuration, which greatly reduces the sensitivity to about $5\,\mathrm{mSLE\,K^{-1}}$. The main contributions stem from the self-sustained advances of the WSB and the WAIS. The latter only experiences a partial regrowth that results from the ice-shelf merger over the Siple Coast, which ultimately leads to a grounding-zone advance limited to this region (Video 5b of the supplementary material). This suggests that the WAIS displays three qualitatively distinct stable configurations: fully covered, collapsed and partially regrown over the Siple Coast. A similar behaviour was simulated in Wirths et al. (2025), albeit with a different spatial pattern.

A number of striking features appear from this analysis. First, the AIS regrowth shows a much more abrupt behaviour than the retreat: whereas the bulk of the volume is recovered via the occurrence of about 15 self-sustained regrowth events (vertical shadings in Fig. 4), gradual ones are largely absent. This means that the sensitivity of volume gain to regional cooling is almost completely determined by the bifurcation points, which display a behaviour that is even more fragmented than during the retreat. Second, these bifurcations seem to be controlled by the bathymetry since they largely happen either in mountain regions or over ocean basins. Therefore, explaining the AIS regrowth largely boils down to understanding how the bathymetry conditions self-sustained advances, which we analyse below.

https://doi.org/10.5194/egusphere-2025-6566
Preprint. Discussion started: 11 February 2026

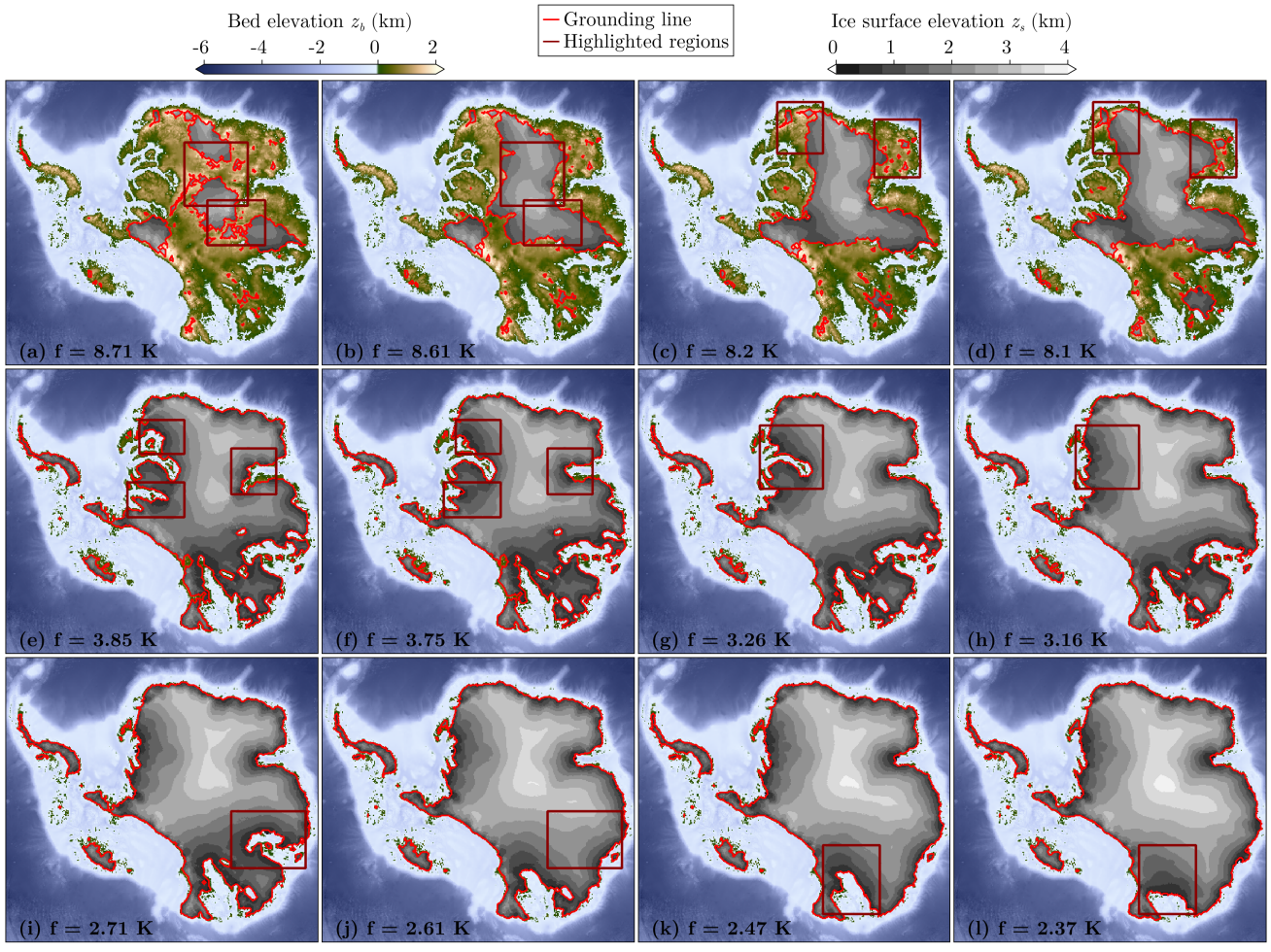

Figure 5. AIS states before and after important bifurcation points of REF highlighted in Figure 4. The regions highlighted by the rectangular frames identify where the regrowth occurs at each bifurcation.

3.2.2 Glacier merger as driver of abrupt regrowth: the perimeter feedback

During regrowth, bifurcations at high temperature anomalies are driven by the merger of previously disconnected ice caps. This is particularly well illustrated in Video 5 of the supplementary material. For instance, at $f = 8.66\,\mathrm{K}$, the ice cap covering the central part of the Gamburstev Mountains merges simultaneously with its eastern part and with the ice cap covering the Queen Maud Mountains, leading to an abrupt volume increase of $3.5\,\mathrm{mSLE}$ (Fig. 4.a-b). We illustrate the physical processes underlying this by depicting some intermediate states of the merger between the Gamburstev and the Queen Maud ice caps. We define the direction connecting them as the normal direction, and, orthogonal to this, the tangential direction. For the present case, they are approximately aligned with y and x, respectively (Fig. 6).

https://doi.org/10.5194/egusphere-2025-6566
Preprint. Discussion started: 11 February 2026

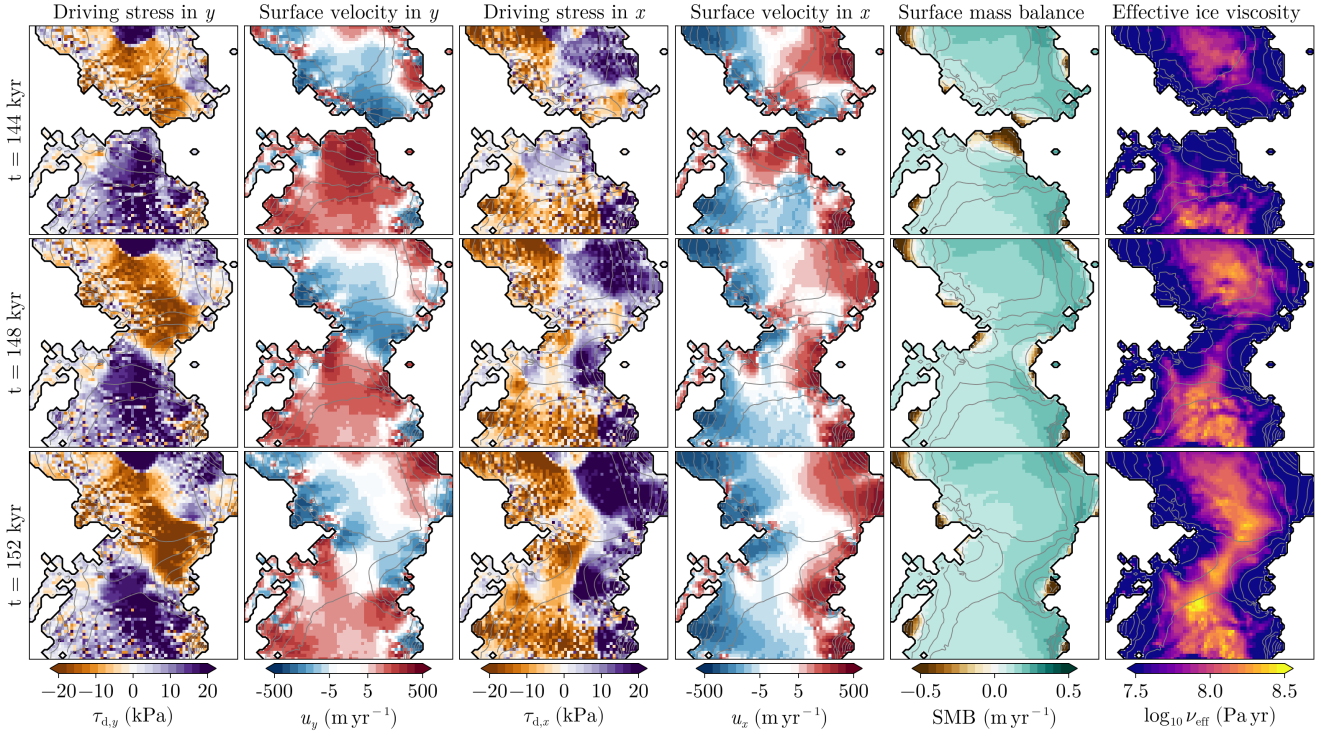

Figure 6. Illustration of the perimeter feedback during the merger of the Gamburtsev and the Queen Maud ice caps, as highlighted in Fig. 5.a-b. The normal and tangential directions largely align along y (vertical) and x (horizontal), respectively. The elevation lines (light gray) show that the merging zone forms a saddle (concave in normal and convex in tangential direction).

The initial configuration, at $t = 144\,\text{kyr}$, is characterised by large surface slopes at the margin of the separated ice caps, which results in high driving stresses and velocities in the normal (y) direction. This leads to high shear stresses, lower ice viscosities and faster flow via the creep feedback (we prefer this denomination over "creep instability" since this process never drives a destabilisation of the AIS in our simulations). In addition, the low surface elevation of the margin implies a negative SMB, which does not favour ice thickening. However, when the two ice caps become connected due to gradual cooling (e.g. at $t = 148\,\text{kyr}$), marginal regions are transformed into interior ones, which greatly reduces their surface slopes, driving stresses and velocities in the normal direction (Fig. 6, column 1-2). In addition, the new interior points are fed by the advection provided by two ice caps instead of one. This favours an ice thickening that is enhanced by two additional processes. On one hand, the melt-elevation feedback transitions from negative to positive SMB values for the cells that were previously covering the margin (Fig. 4, column 5). On the other hand, the reduced velocities imply a decrease in shear stress and therefore an increase in ice viscosity at the newly created saddle (Fig. 4, column 6), which is concave in the normal direction and convex in the tangential one. This profile creates high surface slopes in the tangential (x) direction, thus increasing driving stress and ice flow and easing

https://doi.org/10.5194/egusphere-2025-6566
Preprint. Discussion started: 11 February 2026

the widening of the saddle (Fig. 4, column 3-4). This in turn transforms further marginal regions, characterised by fast flow and negative SMB, into interior ones, characterised by a slower flow and positive SMB, and leads to a self-sustained growth.

We highlight that this feedback essentially arises from a geometric effect (Fig. 7): increasing the surface area of an ice sheet while decreasing its perimeter promotes an increase of mass balance via the dynamic, thermo-mechanic and atmospheric effects explained above. Therefore, we refer to this as the perimeter feedback and propose this denomination to generalise what has been previously described in simulations of rapid ice growth due to saddle mergers (Payne and Sugden, 1990; Bintanja and Van De Wal, 2008; Ji et al., 2021) and rapid ice retreat due to saddle collapses (Gregoire et al., 2012; Gomez et al., 2015; Matero et al., 2017, 2020). As shown in the next subsection, introducing this denomination is an important generalisation since the perimeter feedback plays an important role in self-sustained advances and retreats, even when no saddle collapse or merger takes place.

Within the frame of AIS regrowth, the perimeter feedback is particularly important at high temperature anomalies since the inception starts at topographical peaks, thus creating many neighbouring albeit isolated ice caps. They are characterised by a low area-to-perimeter ratio but can easily merge into larger caps that reduce the overall perimeter while increasing the area. This is similar to merging drops of water: they reduce their contact surface but increase their overall volume, thus fulfilling energy minimisation. The importance of glacier merger for the AIS inception is in line with Payne and Sugden (1990), who described the importance of correctly representing topographic peaks to successfully reproduce the glacial inception of Scotland, driven by the merger of glaciers. Furthermore, the results presented here can be seen as the Antarctic equivalent of the Cordilleran-Laurentide merger described by Bintanja and Van De Wal (2008); Gomez et al. (2015); Ji et al. (2021), although implying smaller volume changes.

3.2.3 Marine perimeter feedback during regrowth

The perimeter feedback applies well beyond the merger of two ice masses, and is equally important when studying the evolution of marine ice sheets. After sufficient cooling, the AIS reaches a configuration that largely follows the coastlines (Fig. 5.e). Grounding-zone advance beyond this is prevented by the comparatively large ocean melt, which leads to an irregular shape of the ice sheet. When the ocean melt is sufficiently reduced, the grounding zone advances and often forms a much smoother front than the coastline, due to continuity. This increases the ratio of interior versus marginal regions, thus reducing melting along the grounding zone and calving at the ice front. The increase in mass balance due to a decreased perimeter can be reinforced by the presence of pinning points and by the occurrence of MISI when retrograde bedrock slopes are reached (often invoked when studying retreat, but equally applicable to regrowth, as shown in Schoof (2007); Moreno-Parada et al. (2025)). The combination of these effects is responsible for the self-sustained regrowth of the AIS over marine-based regions, which characterises the equilibrium diagram at low temperature anomalies (Fig. 5).

An instance of this is provided by the ASB, where ice first advances over a pinning point (Fig. 8, from $t = 574$ until $t = 577\,\mathrm{kyr}$). This reduces the perimeter of the grounding zone (approximated by the cell count, Fig. 8.c) and therefore the associated total BMB (Fig. 8.a), even though the regionally averaged BMB becomes more negative (Fig. 8.b) due to the exposure to higher ocean temperatures. The reduction of the total BMB at the grounding zone leads to an advance of the

https://doi.org/10.5194/egusphere-2025-6566
Preprint. Discussion started: 11 February 2026

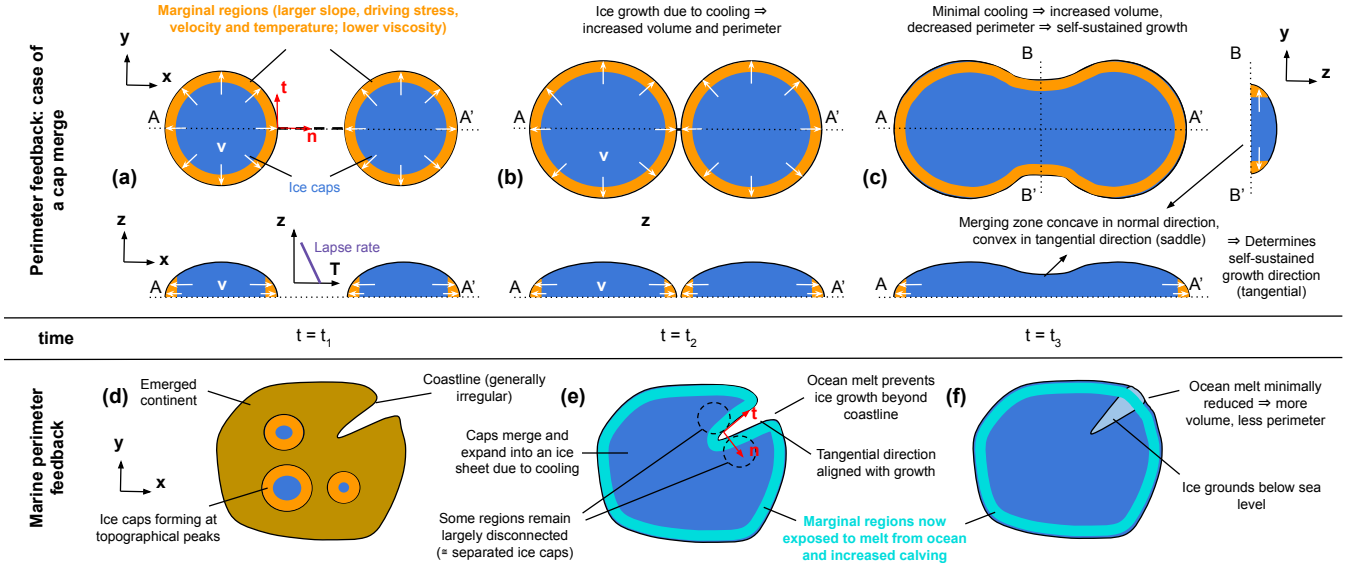

Figure 7. Schematic representation of the perimeter feedback, where $\boldsymbol{n}, \boldsymbol{t}$ represent the normal and tangential directions, respectively. (a-c) When two ice caps merge, the extent of marginal regions, which are faster-flowing ablation zones, is reduced. The flow at the coalescence zone is re-oriented from the normal to the tangential direction via the formation of a saddle. This leads to a widening of the saddle in this direction and a further reduction of the perimeter, thus starting a positive feedback loop. (d-f) After an inception dominated by the merger of ice caps, the ice sheet reaches coastlines, beyond which grounding zone advance is prevented by ocean melting. This leads to an irregular shape and a large perimeter of the ice sheet, subject to enhanced melting and calving at its margin due to the contact with the ocean. The regions on both sides of an ocean basin are connected via remote interior regions but can be seen as disconnected from a local perspective. When ocean melt is sufficiently reduced, the grounding zone advances and leads to a reduction of the perimeter via continuity, starting a positive feedback loop which ends with a much reduced ratio of perimeter to surface area.

marine basin, which further reduces the grounding-zone perimeter and drives a self-sustained regrowth. At the end of this, the grounding-zone perimeter is reduced by a factor 3. A similar behaviour is simulated for the BMB of ice shelves and for calving, which both become more negative on average but are reduced overall due to the conversion of many floating cells into interior ones (Fig. 8). This mechanism applies to the regrowth of all EASBs and is also illustrated for RSB, where the grounding-zone advance "zips" the ice on either side of the basin together (Fig. D4).

Distinguishing the contributions of the perimeter feedback versus MISI is complicated since they lead to similar changes (e.g. decreased velocity and BMB at the margin) and none of them can be deactivated independently of each other in simulations. Analysing metrics that characterise MISI and the perimeter feedback does not allow comparing them directly but reveals that the perimeter feedback is more important during the regrowth of marine basins than during their retreat, whereas MISI metrics are larger during retreat compared to regrowth (Fig. C1). This can be explained by the fact that, on one hand, the regrowing AIS shows a much more irregular shape than its retreating counterpart (e.g. Fig. 2.f vs. Fig. 5.e), allowing for a larger effect of the perimeter feedback. On the other hand, retrograde bed slopes below sea level are much rarer at an intermediate regrowth

https://doi.org/10.5194/egusphere-2025-6566
Preprint. Discussion started: 11 February 2026

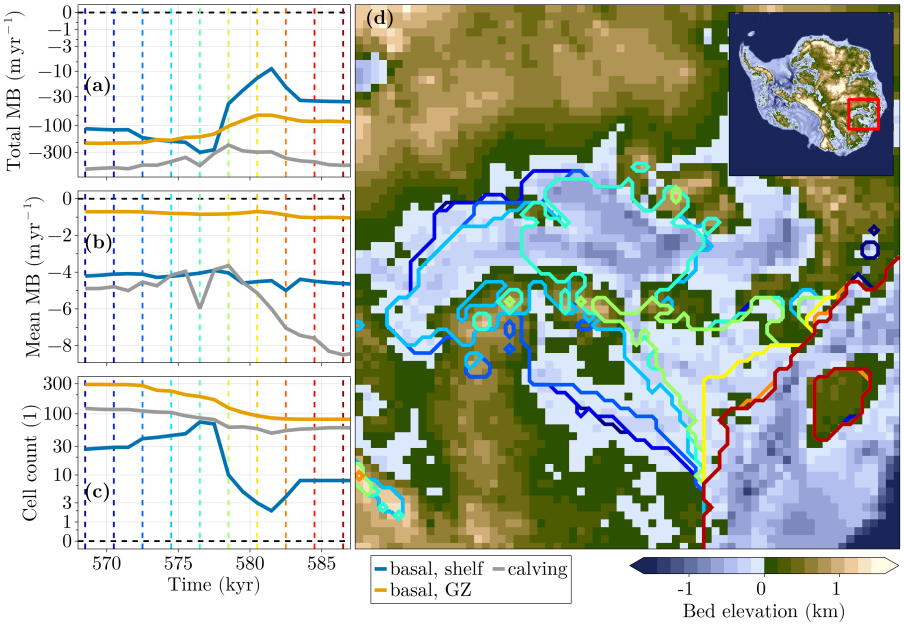

Figure 8. Perimeter-driven regrowth of the ASB. (a-c) The total MB becomes more positive although the mean MB becomes more negative, due to the strong decrease of ice-shelf area, grounding-zone length and calving front length via the perimeter feedback. (d) The onset of the latter is eased by a pinning point and a very irregular shape of the ASB, prior to the transition.

stage, thus reducing the retrograde character of the Antarctic bed (Fig. 9 and B1) and therefore the likelihood of MISI. This can be explained by the fact that the AIS only extends until the coastlines and that the marine, ice-free regions therefore have not undergone a bedrock depression due to isostatic adjustment yet. In contrast, the bathymetry equilibrated with the present-day AIS presents retrograde bedrock slopes that are much more marked (Fig. 9 and B1). This is mostly due to the fact that ice is thicker towards the interior, leading to a differential bedrock displacement, i.e. a larger bedrock depression in the interior compared to marginal regions. This highlights an important effect: when solely considering an immediate AIS state, GIA appears to be a negative feedback on ice retreat via bedrock uplift. However, when taking into account the AIS history, GIA largely facilitates MISI due to the retrograde slopes created by the differential bedrock depression resulting from the existence of the AIS itself. This already highlights the importance of the bathymetry, which is studied in greater detail in the next subsection.

3.2.4 On the importance of bathymetry

Remarkably, not all the bifurcations of the retreat branch have their counterpart in the regrowth branch, and vice-versa. For instance, the retreat in the EAIS interior is not marked by many saddle collapses (Fig. 1), although the regrowth is dominated by glacier mergers (Fig. 4). This asymmetry in bifurcations appears to be a consequence of the irregular bathymetry, but confirming this would require a set of idealised experiments that are left for future work.

https://doi.org/10.5194/egusphere-2025-6566
Preprint. Discussion started: 11 February 2026

In spite of this general lack of symmetry between retreat and regrowth, most of the abrupt EASB regrowths are comparable to the ones occurring during retreat. In some cases, the order of regrowth mirrors that of the retreat. For instance, the Pensacola-Pole basin is the last to collapse and the first to regrow. This can be attributed to (1) the narrow, fjord-like structure of the basin that eases the perimeter feedback, (2) the existence of numerous islands that provide pinning points and retrograde slopes for MISI to take place and (3) the vicinity to the South Pole, providing low temperatures. When considering the bathymetry during regrowth, it appears that (1) and (2) are significantly reinforced by the GIA response to the previous deglaciation (Fig. 9). Conversely, the WSB is the first EASB to collapse and the last to regrow due to (1) the wide structure of the basin that complicates the onset of the perimeter feedback, (2) a sparse island coverage providing few pinning points and retrograde slopes and (3) some of the highest temperatures in East-Antarctica due to the remoteness to the South Pole. Here the GIA response plays a significant role in reducing the basin size but is not capable of producing a narrow structure or numerous islands. The latter can be greatly altered by the resolution of the bathymetry and the GIA model (Fig. 9 vs. Fig. B1).

However, the mirrored bifurcation order of Pensacola-Pole and Wilkes seems to be an exception. For instance, the ASB is the last major basin to collapse (at $f = 8.6\,\mathrm{K}$, Fig. 1) but is also one of the last basins to be recovered (at $f = 2.6\,\mathrm{K}$, Fig. 4). The former can be explained by the fact that many islands prevent the grounding zone from reaching the retrograde portion of the bed during the retreat, thus only allowing MISI at high temperature anomalies. The latter can be explained by the width and the pronounced coastline irregularity of the basin, which significantly complicates the onset of a perimeter-driven regrowth (Fig. 8). This illustrates that it is generally wrong to assume that the regrowth mirrors the retreat, mostly because the bathymetry in the vicinity of the grounding line can be drastically different between the AIS retreat and regrowth. This is due to the different grounding-zone position prior to the onset of positive feedbacks (e.g. Fig. 2.g versus Fig. 5.f) and to the differences in bedrock elevation modulated by GIA (Fig. 9 and Fig. B1).

Remarkably, the volume gain associated with each grounding-zone advance tends to be larger than its counterpart from the retreat branch. For instance, the ASB collapse implies an ice loss of $3\,\mathrm{mSLE}$, whereas its recovery implies an ice gain of $7\,\mathrm{mSLE}$. This can be explained (1) by the larger impact of the perimeter feedback at regrowth which is due, as mentioned above, to the stronger irregularity of the margin (Fig. 8) and (2) by the fact that the EASBs are not recovered at all unless the GMT anomaly is much lower than the corresponding bifurcation point of the retreat, which implies a larger accumulation.

We propose to further quantify the importance of the bathymetry by running two additional regrowth experiments, UPL and DPR. In both cases, the vertical bedrock displacement is deactivated and the bathymetry is held constant in its uplifted configuration (UPL, in equilibrium with an ice-free continent) or in its depressed configuration (DPR, in equilibrium with the present-day configuration). Compared to the depressed bathymetry, the uplifted one presents a drastically reduced extent of marine regions, as particularly observed in the east (Fig. 9). In addition, many bathymetric peaks below sea level become islands, as observed in the WAIS, where archipelagos arise. As discussed in Sec. B, these features can be affected by the resolution and are key for the regrowth process, since islands provide retrograde slopes and pinning points that prevent ocean melt, therefore easing the grounding-zone advance in marine regions.

As depicted in Fig. 4, the regrowth of REF and UPL barely show any differences. This means that, at equilibrium, the original bedrock elevation is a much stronger control on regrowth than the subsequent bedrock adjustment. In contrast, DPR

https://doi.org/10.5194/egusphere-2025-6566
Preprint. Discussion started: 11 February 2026

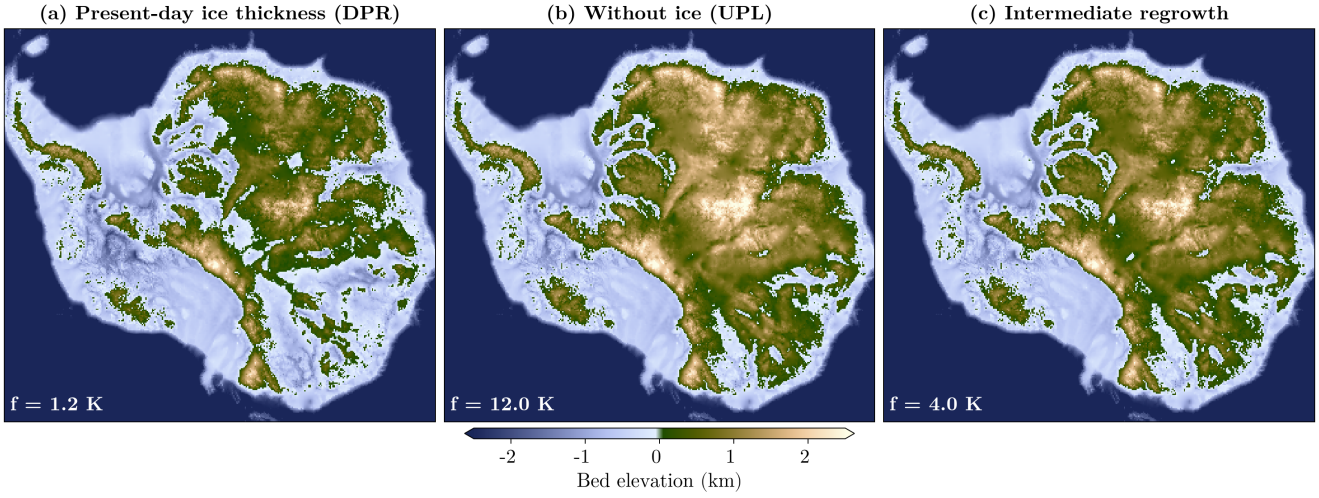

Figure 9. Antarctic bedrock elevation in equilibrium with (a) the present-day ice thickness (DPR), (b) an ice-free continent (UPL), and (c) the intermediate regrowth stage at $f = 4\,\mathrm{K}$. Remarkably, DPR presents marine basins that are drastically larger than in UPL due to the bedrock depression implied by the presence of thick ice. In contrast, the marine basins shown in (c) only marginally differ from those of UPL because ice has not advanced over the marine basins yet, implying a negligible bedrock adjustment. This is further reinforced by the very irregular shape of the ice sheet, which is unable to grow thick ice at the coastlines due to the large ratio of marginal over interior points (e.g. Fig. 3.f).

is qualitatively similar to REF but shifted towards lower temperatures. At high temperature anomalies, this discrepancy can be explained by the fact that the mountains, where inception begins, are less elevated in DPR and are thus exposed to higher air surface temperatures. Therefore, ice regrowth only starts at $f < 7\,\mathrm{K}$ in DPR, whereas it already starts at $f < 9\,\mathrm{K}$ in UPL and REF. At low temperature anomalies, the discrepancy mostly arises from marine topography: compared to REF and UPL, DPR shows less islands and wider regions of bedrock below sea level (Fig. 9), which prevents the regrowth over marine regions. For the lowest temperature anomalies, ocean melt in the east becomes almost negligible and, remarkably, all EASBs readvance at the same time (Video 8 of the supplementary material), which gives rise to an even more abrupt regrowth than what is observed in REF. Counter-intuitively, the final volume of REF is larger than UPL. This can be explained by the fact that a deeper bathymetry allows for more volume, given a fixed ice-sheet extent. This also partly explains why DPR displays a larger volume than REF at $f = 0\,\mathrm{K}$, which is additionally reinforced by the fact that the WAIS grounding zone does not only advance over the Siple Coast, but also towards the Amundsen Sea Embayment (Video 5, 7 and 8 of the supplementary material). This appears to be the case because the advection of ice is stronger in DPR, thus leading to the formation of ice shelves on both sides of the Amundsen Sea Embayment, which manage to merge and thus drive a stronger advance of the WAIS. The stronger advection of DPR is likely explained by deeper bed implying larger ice thickness at the grounding zone, which is a nonlinear control of the outflow at the grounding zone (Schoof, 2007).

https://doi.org/10.5194/egusphere-2025-6566
Preprint. Discussion started: 11 February 2026

Generally, the uplifted bedrock of REF and UPL reduces the extent of marine basins, which reduces the amplitude of the tipping. Furthermore, it reduces the connectivity between two basins and therefore prevents a propagation of instabilities from one region to the other, thus increasing the fragmented nature of the regrowth curve, which is significantly more marked for REF and UPL than for DPR. This is similar to what was described above for REF and DPR during retreat.

3.2.5 Conclusions on the equilibrium AIS regrowth

In summary, the equilibrium behaviour of the AIS regrowth, marked by even more bifurcations than the retreat, can be well resolved by the AQEF. Its sensitivity is mostly controlled by the occurrence of self-sustained advances that result either from saddle mergers or from grounding-zone advances over marine basins, which are both subject to the perimeter feedback. The latter is more important during regrowth than during retreat, whereas MISI is more important during retreat than during regrowth. Remarkably, the AIS regrowth is characterised by a long phase of almost zero sensitivity to cooling, when the ice sheet has already reached most coastlines but is incapable of advancing beyond, mostly due to their irregular shape that implies a large perimeter. This stresses the important control of the bathymetry on AIS regrowth, which is modulated by the GIA response. In particular, the uplifted AIS bathymetry facilitates mass gain for most of the temperature range, except for low GMT anomalies where a depressed bathymetry appears more efficient for ice regrowth, likely due to the stronger advection that result from it in marine regions.

3.3 Hysteresis and comparison to previous studies

After considering the retreat and regrowth separately to better highlight the underlying mechanisms, we now compare them to quantify the hysteresis effect. In this section, we first study what are the main controls on the hysteresis. Then, we put this into perspective by comparing our results to those obtained by studies with a similar simulation setup. Finally, we investigate how regrowing from intermediate retreat states affects the hysteresis and provide practical insights to inform decision-making with respect to future global warming. For each shared socioeconomic pathway (SSP, Riahi et al., 2017), we define $\bar{f}$ and $\hat{f}$ as the best estimate and the maximum of GMT anomaly by 2100, respectively.

3.3.1 Main controls of the hysteresis

To analyse the hysteresis, we define its width as the temperature difference between retreat and regrowth for a given volume, and its height as the volume difference between retreat and regrowth for a given temperature. These independent metrics characterise how irreversible and how large a given sea-level contribution is.

Since $f_o = 0$ in ATM, this experiment yields the smallest sensitivity with respect to ocean warming across the permutations presented here (Fig. 10). REF yields a larger sensitivity and DPR an even larger one, due to a larger ocean connectivity resulting from the absence of isostatic uplift. The height and particularly the width of the hysteresis seem to follow the order of the ocean sensitivity: these metrics are smallest for ATM, large for REF and even larger for DPR. This points out that ocean melt, modulated by the bathymetry, is an important control on the hysteresis width, partly due to its importance for MISI and

https://doi.org/10.5194/egusphere-2025-6566
Preprint. Discussion started: 11 February 2026

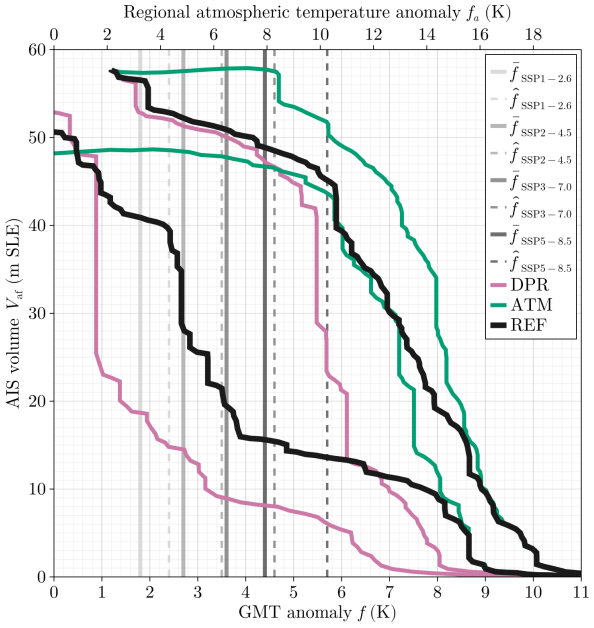

Figure 10. Comparison between the AIS hysteresis diagrams obtained in the present study (reference run, REF; atmospheric forcing only, ATM; depressed bedrock configuration, DPR) and the warming at year 2100 for various SSP scenarios.

the perimeter feedback. OCN is excluded from Fig. 10 because its regrowth is completely prevented by the lack of increased precipitation, due to the lack of atmospheric warming. We note that refreezing is not allowed, which is plausible for the range of GMT anomalies studied here. This suggests that ocean melt is an important positive control on hysteresis width while the precipitation feedback is an important negative control. We note that UPL is excluded from this analysis because its retreat would require a distinct spin-up, which prevents a one-to-one comparison.

3.3.2 Comparison to previous studies

After comparing various simulation setups within our frame of study, we propose to compare our results to the literature (Fig. 11). Two previous studies analysed the hysteresis of the AIS in the absence of the melt-albedo feedback. For the rest of this section, we refer to them as H94 (Huybrechts, 1994) and G20 (Garbe et al., 2020). H94 was limited to the study of grounded ice forced by atmospheric warming. It is therefore outdated in terms of complexity but provides insights nonetheless since it is similar to ATM, however excluding oceanic melt and MISI. In spite of these differences, H94 and ATM present many similarities. In both retreats, the ice volume first increases before reaching a phase of strong decrease. However, ATM is marked by abrupt retreats driven by MISI, which are absent from H94 and are likely responsible for the somewhat larger hysteresis of ATM.

https://doi.org/10.5194/egusphere-2025-6566
Preprint. Discussion started: 11 February 2026

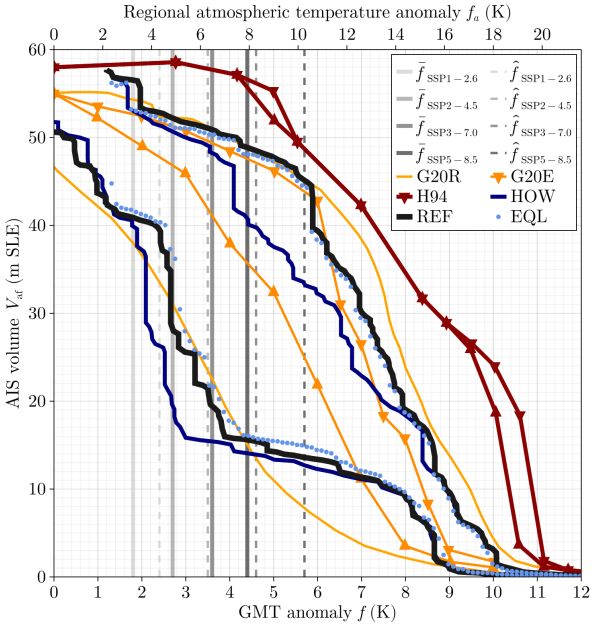

Figure 11. Comparison between some AIS hysteresis diagrams obtained in the present study (reference run, REF; branched-off equilibrium results, EQL; high ocean warming, HOW) and results obtained in H94 (Huybrechts, 1994) and G20 (Garbe et al., 2020, distinguished between runs applying slow forcing ramps, labelled G20R, and branched-off equilibrium runs, labelled G20E).

In contrast, G20 largely resembles the simulation setup of REF. It however differs from the present study in three major ways. First, G20 uses a scaling of $f_o = 0.39 \cdot f_a$ between the regional atmospheric and oceanic warming, based on a long-term simulation of MPI-ESM. For REF, we prefer to rely on the aforementioned factor of 0.25 derived from an ensemble mean, but, to allow comparisons, we also perform a retreat experiment with 0.39, called HOW (high ocean warming). Second, G20 uses a power law with exponent 0.75 to describe basal friction. This results in a quasi-linear dependence between basal friction and velocity, which, unlike the regularized Coulomb law used here and inferred from laboratory experiments (Zoet and Iverson, 2020), does not saturate at high velocities (Fig. A1). In G20, if the base of the ice is not lubricated, any acceleration of fast-flowing streams is therefore partly compensated by an increase in basal friction, potentially reducing the outflow. Third, no melt is applied at the grounding line but a flux condition is imposed. This is not in line with recent observations of tidal water intrusion beyond the flotation criterion (Christianson et al., 2016; Chen et al., 2023; Rignot et al., 2024, e.g.) and leads to a reduced sensitivity to ocean warming compared to PMPT, used in our setup. In addition to these differences in parametrisation, G20 uses a finer horizontal resolution of $\Delta x = 8\,\mathrm{km}$, which only marginally affects the results compared to a run with $\Delta x = 16\,\mathrm{km}$ (Garbe et al., 2020). In the present study, the ice dynamics is solved with DIVA instead of the hybrid SSA/SIA used in G20 since it was shown to be a better approximation of Stokes flow (Robinson et al., 2022).

To obtain the equilibrium diagram, G20 uses ramp experiments from which equilibrium runs are branched off. We refer to these runs as G20R and G20E, respectively. Whereas G20R and G20E are relatively similar for the retreat branch, they are

https://doi.org/10.5194/egusphere-2025-6566
Preprint. Discussion started: 11 February 2026

very different for the regrowth one. For instance, at $f = 5\,\mathrm{K}$, the volume difference between both yields as much as $22\,\mathrm{mSLE}$. This difference is much more than what is found between REF and EQL (Fig. 7), which yields $1\,\mathrm{mSLE}$ on average, with peak values of a few metres in the vicinity of bifurcations. This points out that AQEF approximates the true equilibrium much closer than ramp experiments. This is mostly due to the adaptive nature of the technique, which stops forcing when the ice volume changes faster than tolerated.

The quantitative similarities between the retreat curves of REF and G20E are striking. It should however be stressed that they deliver qualitatively different insights. Strictly speaking, G20 shows a bifurcation for the WAIS, but not for the EASBs and EAIS. The continuously resolved forcing space of REF however provides a totally different view: whereas the WAIS is, in fact, characterised by a single tipping point, the EASBs are characterised by many individual tipping points of various amplitudes and very distinct forcing levels, while the EAIS shows two bifurcation points of small amplitude, associated with the aforementioned saddle collapses. However, it should be emphasised that no threshold for the EAIS interior can be reliably given without the inclusion of the melt-elevation feedback. Therefore, at high temperature anomalies, the bifurcation point simulated by Leloup et al. (2025) should be preferred to the values obtained in G20 and in the present study.

Interestingly, G20E, HOW and REF converge to the similar values for $f > 7\,\mathrm{K}$. This confirms that, in this part of the diagram, ice retreat is dominated by the melt-elevation feedback, which is similarly represented in all experiments. This robust feature remarkably aligns with paleoclimate evidence, which suggests that Antarctica has never been ice-free since around 34 million years ago (Miller et al., 2020), when global mean surface temperatures were around 6–8°C warmer compared to the pre-industrial average (Westerhold et al., 2020).

For the regrowth curves, REF and G20E show important differences, both qualitatively and quantitatively. Whereas G20E shows an almost constant sensitivity, REF shows very distinct phases, as described above. This includes a phase of almost zero sensitivity, which corresponds to the long forcing range where the AIS is incapable of advancing over marine regions (Fig. 4-5). This difference might be explained by the enhanced ocean sensitivity and the reduced friction resulting from the use of PMPT and a regularised Coulomb law, respectively. This discrepancy in the regrowth curve is responsible for the larger hysteresis simulated here, compared to G20. Whereas G20E yields a maximal hysteresis of $2.5\,\mathrm{K}$ and $20\,\mathrm{mSLE}$ in width and height, respectively, REF yields maximal values of about $4.5\,\mathrm{K}$ and $35\,\mathrm{mSLE}$. Here, the magnitude of the hysteresis, especially its width, increases with increasing sensitivity to ocean warming: H94 is not sensitive to ocean temperatures (only grounded ice is represented) and displays a very narrow hysteresis; G20 shows an intermediate ocean sensitivity and wide hysteresis; REF presents a large ocean sensitivity and very wide hysteresis; HOW presents the largest ocean sensitivity and the widest hysteresis. As hypothesised above, this suggests that, in the absence of melt-albedo feedback, ice-ocean interactions, which are modulated by the coastline shape, are the main source of irreversibility. Including melt at the grounding zone aligns with observations and yields an ocean sensitivity that implies a larger hysteresis of the AIS, compared to what was previously assessed in similar frameworks.

https://doi.org/10.5194/egusphere-2025-6566
Preprint. Discussion started: 11 February 2026

3.3.3 Practical implications and regrowth from intermediate retreats

REF and HOW present bifurcation points of the WAIS that are situated between the values obtained in Van Den Akker et al. (2025) and Garbe et al. (2020), therefore representing intermediate values within the literature. Regardless of the ocean sensitivity assumed, the bifurcation point of the WAIS simulated here is overshot by any realistic projection at year 2100. Although overshooting a bifurcation point does not necessarily imply triggering it (Bochow et al., 2023), projections show that tipping of the WAIS (Seroussi et al., 2024; Klose et al., 2024; Coulon et al., 2024, 2025; Van Den Akker et al., 2025) is likely to happen over the coming millennium. An associated key question is to understand what level of cooling would be needed to regrow the WAIS after such an event. However, until now, studies of the AIS hysteresis have only performed regrowth experiments from a completely collapsed AIS, a situation that is a-priori quite unrelated to the question above. To address this, we run regrowth experiments from various stages of the retreat (Fig. 12). Interestingly, most of these experiments yield a horizontal line in the hysteresis diagram, until the regrowth branch is reached and subsequently closely followed. This means that the regrowth curve from an ice-free Antarctica is a quite good proxy for the AIS regrowth from intermediate stages.

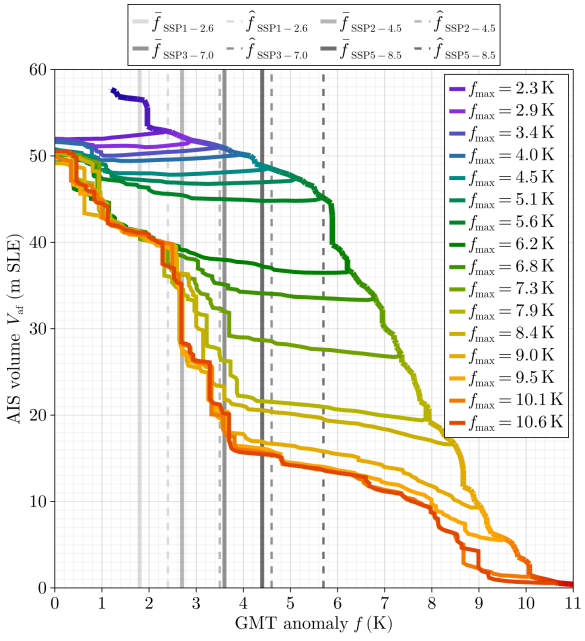

Figure 12. AIS hysteresis diagram when regrowing from various intermediate warming levels.

However, the additional curves obtained here yield complementary information. For instance, reducing the GMT anomaly from 2.3 K (slightly warmer than the WAIS bifurcation point) to 0 K (pre-industrial GMT) leads to a further decrease of the ice sheet volume by an additional metre of sea-level equivalent. This might appear unintuitive but can be explained. On one hand, although ocean temperatures are decreasing, they are not sufficiently cold to allow a WAIS regrowth. On the other hand, reducing atmospheric temperatures leads to a reduction of accumulation, leading to net volume loss. This is important since it

https://doi.org/10.5194/egusphere-2025-6566
Preprint. Discussion started: 11 February 2026

means that the path to a complete WAIS regrowth likely requires intermediate configurations that imply an even larger sea-level contribution of as much as $1\,\mathrm{mSLE}$. Since the WAIS is not regrown at pre-industrial GMT, our simulations suggest that if the WAIS tips, human societies would be committing to a sea-level rise of $3.5 - 4.5\,\mathrm{mSLE}$ that is irreversible in practical terms, since cooling the climate below pre-industrial level is unlikely and would probably have other undesired impacts.

When assuming an intermediate ocean warming (REF), none of the scenarios reach the bifurcation point of the WSB by 2100 (Fig. 10-12). However, since the high-emission scenarios (SSP3-7.0 and SSP5-8.5) come close to this value and present significant warming trends at the end of the century, they would likely overshoot this bifurcation point over the 22nd century, as in numerous ensemble members of Seroussi et al. (2024); Klose et al. (2024); Coulon et al. (2024, 2025). Recovering the WSB requires GMT anomalies of $f < 1\,\mathrm{K}$, i.e. a climate that is colder than the present-day one (Fig. 12). Thus, a future retreat of the WSB, or any other EASB, is likely irreversible in practical terms (12). This suggests that a committed AIS contribution of $18\,\mathrm{mSLE}$ cannot be ruled out if the GMT anomalies of the high-emission scenarios are maintained long enough, or if the sensitivity of the Southern Ocean to global warming is larger than expected (HOW, Fig. 11). Most importantly, as described in Sec. 3.1, collapsing the WSB initiates a phase of large sensitivity, where increasing GMT by one degree implies an equilibrium ice loss of $11.5\,\mathrm{mSLE}$. To put these number in perspective, about a billion humans live between 0 and 10 metres above global mean sea level. This points out that ice retreat does not need to be self-sustained to have catastrophic implications for the adaptability of human societies. In addition, a collapse of the WAIS and, to a smaller extent, of the WSB, would drastically reduce the ice-covered surface area and therefore the mean regional albedo, leading to a larger polar amplification than the constant factor of 1.8 assumed here. This could amplify the contribution to sea-level rise and might imply cascading effects, both within the AIS and for the whole Earth system.

4 Discussion

The retreat experiments shown in Sec. 3.1 highlight that MISI is a significant driver of EAIS retreat. This is an important contrast to what was described in other studies of the AIS hysteresis (Huybrechts, 1994; Pollard and DeConto, 2005; Garbe et al., 2020; Van Breedam et al., 2023; Leloup et al., 2025), where EAIS ice loss was largely attributed to feedbacks linked with the atmosphere and the energy balance. However, Garbe et al. (2020, c.f. video of AIS retreat provided as supplementary material) also showed abrupt retreats of the EASBs, similar to those observed here. We believe that this is not described in the manuscript because the use of offline forcing techniques precludes the identification of the bifurcation points. The computation of mass balance contributions is performed over the whole domain, which can hide regional peak contributions of basal melt, unlike the regional analysis shown in Fig. 2. We point out that the equilibrium retreat obtained here is therefore qualitatively similar to Garbe et al. (2020) but the interpretation differs.

The perimeter feedback was illustrated on the regrowth branch of the AIS but conversely applies to ice retreat, as shown by the peaking perimeter metric in most of the self-sustained retreats (Fig. C1). Of course, this applies to the saddle collapses simulated at high GMT anomalies in the EAIS (Fig. D2), but is also a key process to explain why the retreat of marine ice sheets is not limited to the retrograde portion of the bedrock (Fig. D1, where the interplay of MISI and the perimeter feedback

https://doi.org/10.5194/egusphere-2025-6566
Preprint. Discussion started: 11 February 2026

is illustrated in greater detail for the WAIS collapse.). First, MISI drives the retreat and thus largely follows the retrograde bedrock. This leads to a grounding zone and a shelf geometry that is much more irregular than prior to MISI, therefore increasing the perimeter and the total ocean melt and calving. This causes the grounding zone to retreat further until reaching an equilibrium between the advection of upstream ice and the ablation that is characteristic of marginal regions. To a first order, this means that MISI determines where the instability begins (and therefore the associated bifurcation point), whereas its interplay with the perimeter feedback determines where it ends (and therefore the amplitude of the bifurcation), while both are conditioned by the bathymetry and therefore by potential GIA effects.

Sometimes, an occurrence of MISI can sufficiently affect the ice-sheet geometry to drive the onset of a saddle collapse, as in the case of the ASB retreat (Fig. 2.g-h). First, MISI greatly reduces the connectivity of Adélie Land to the rest of the AIS, thus increasing the perimeter. This triggers a larger outflow, lower ice viscosities and a decrease in SMB, ultimately leading to the separation of the two regions which retreat even more due to the increased perimeter (Fig. D2). This is very similar to what is described by Gregoire et al. (2012), who suggest that, during the last deglaciation, the separation of three domes of the Laurentide Ice Sheet could have led to large sea-level contributions. These domes reached over Hudson Bay, which, even without MISI, can provide a mechanism to split the domes via ocean melt. The similarity with the split simulated in the ASB, which is also initiated by increased ocean melt, is therefore striking.

To date, only one other study has investigated the role of GIA on the AIS hysteresis (Van Breedam et al., 2023). Comparisons with our work are however difficult since the bathymetry used by Van Breedam et al. (2023) aims to reproduce the conditions of the Early Cenozoic and assumes a bedrock below Antarctica that is almost completely emerged, thus preventing interplays between GIA, MISI and the marine perimeter feedback. GIA is generally understood as a net negative feedback on ice sheet dynamics (e.g. Gomez et al., 2012; Whitehouse et al., 2019; Gomez et al., 2024). However, exceptions to this understanding arise. For instance, simulations of the last glacial cycle have shown that the peripheral forebulge that rises around a subsiding region can form retrograde slopes, leading to a positive feedback between GIA and MISI (Albrecht et al., 2024). This is likely to have eased the advance of the Ross and Filchner-Ronne grounding zones until the continental shelf break. Along a similar line of thought, our study demonstrates that the presence of a fully developed AIS leads to significant retrograde slopes and larger oceanic basins, which are key for the simulated MISI-driven retreats. Conversely, the small bed depression simulated at intermediate regrowth stages eases the occurrence of self-sustained regrowth. Unlike what is described by Albrecht et al. (2024), these are not strictly speaking positive feedbacks but reinforce other positive feedbacks when taking into account the coupled AIS-GIA history.

In the present study, the melt-albedo feedback is not represented, although it was shown to be the driver of complete ice retreat/regrowth once the AIS extent is small/large enough. This was observed when representing the coupling of the AIS to the climate via a matrix method (Pollard and DeConto, 2005), a climate emulator (Van Breedam et al., 2023) or an Earth model of intermediate complexity (Leloup et al., 2025), and therefore appears to be a robust feature. In the present study, the absence of this coupling has enabled cheaper simulations and, most importantly, the identification of processes that were previously underestimated (MISI is not only operating in the WAIS) or even absent from literature on the AIS hysteresis (the perimeter feedback is important for the AIS retreat and particularly its regrowth).

https://doi.org/10.5194/egusphere-2025-6566
Preprint. Discussion started: 11 February 2026

Whereas the melt-albedo feedback can reinforce these processes, we point out that it can conversely be reinforced by them. For instance, prior to the abrupt ice regrowth driven by the melt-albedo feedback, Van Breedam et al. (2023) show a proto-AIS that is disconnected but very close to a smaller ice cap covering the Transantarctic mountains, showing remarkable similarities to the situation shown in Fig 5.b-c. We suspect that, for a minimal decrease of temperature, these caps merge, which abruptly increases the ice-covered surface area due to the perimeter feedback and triggers the melt-albedo feedback, leading to an almost fully ice-covered continent. Another example of this is that, in the work of Leloup et al. (2025), the onset of the full AIS retreat, driven by the melt-albedo feedback, coincides in time with the end of what appears to be a MISI-driven retreat of the WSB. This suggests that the bare rock and ocean, exposed by the retreat, reduce the albedo sufficiently for the melt-albedo feedback to be triggered. Of course, these specific observations need more investigation to be confirmed, but we want to emphasise the underlying, more general idea: MISI, the melt-elevation, the melt-albedo and the perimeter feedbacks can trigger each other. This implies that the representation of one process can greatly influence the bifurcation induced by another one through a cascading effect. Tipping cascades usually refer to the destabilisation of a tipping element triggered by the tipping of another one. We here emphasise that the AIS is a spatially heterogeneous system with several sub-components, each of them presenting a distinct bifurcation point, that can be seen as interacting tipping elements. For instance, as seen in the comparison between the REF and DPR retreat, many basins retreat in two steps if GIA is active, but only in a single one if GIA is deactivated. In particular, the interior of the EAIS and the EASBs present important interplay that can lead to joint tipping events, as shown in Fig. D2.

Assuming a constant polar amplification factor as done here is not realistic since the surface covered by grounded, floating and sea ice is an important control of the energy balance at high latitudes via the albedo feedback. Nonetheless, we point out that simulations including this feedback produce regional atmospheric temperatures between 15 and $20\,\mathrm{K}$ at the end of the AIS collapse (Van Breedam et al., 2023; Leloup et al., 2025). When applying a polar amplification of 1.8 or a realistically somewhat larger factor, this corresponds to the range simulated here (Fig. 10).

Furthermore, our results can shed some light on future projections: ungrounding the major EASBs via MISI is relatively unlikely over the coming millennium but is associated with grounding line retreats that reach deep into the interior of the EAIS (Klose et al., 2024; Coulon et al., 2024, 2025), which is consistent with the bifurcation points assessed here. This also aligns with the multistability of EASBs assessed in Wirths et al. (2025), which paced the AIS volume changes during the whole Pleistocene via abrupt retreats and regrowths.

The present study shows clear limitations: (1) the resolution of the grounding zone is too coarse to obtain quantitatively reliable estimates of the bifurcation points associated with MISI, (2) the melt-albedo feedback is not represented, (3) many parametric uncertainties are not explored, (4) PMPT could be replaced by a more comprehensive approach (e.g. Ross et al., 2024) and (5) subglacial hydrology is treated locally, although the large temperature anomalies explored here would lead to a significant re-routing of subglacial water flow. Most of these limitations are due to the prohibitive computational cost of the experiments, which are conditioned by the large simulation time needed to obtain equilibrium states (about $15\,\mathrm{Myr}$ in total for this study). We emphasise that these limitations are important if quantitative values are to be robustly assessed. This is however not the aim of this study, which focuses on the mechanistic explanation of self-sustained retreat and regrowth events, as well

https://doi.org/10.5194/egusphere-2025-6566
Preprint. Discussion started: 11 February 2026

as their impact on the shape of the AIS hysteresis. Nonetheless, we stress that the simulation setup verifies many sanity tests: the present-day state is close to the observed one and the retreat/regrowth behaviour appears plausible. In particular, the WAIS retreat is initiated in Thwaites and the AIS regrowth takes place from the interior towards the margin of the continent.

5 Conclusions

In the present study, an adaptive, online forcing technique was introduced to obtain an AIS equilibrium diagram that is continuously resolved over the forcing space and yields results that, compared to the offline forcing techniques used to date, are much closer to equilibrium. Most importantly, this technique is more accurate at capturing self-sustained changes of the AIS volume, which are found to be more numerous than what was previously shown in similar studies. For most of the bifurcations during the AIS retreat, the underlying process has been identified to be MISI, which, besides taking place in the WAIS as already demonstrated (e.g. Garbe et al., 2020; Leloup et al., 2025), also takes place in the EASBs. This is facilitated by the large GIA slopes induced by the presence of an ice sheet that is thicker towards the interior. The perimeter feedback is often triggered by the onset of MISI and explains why grounding-zone retreat might continue over regions with a prograde bedrock. Furthermore, the perimeter feedback was identified as an important driver of self-sustained AIS regrowth at high temperature anomalies, mostly due to important mergers between ice caps. At lower temperature anomalies, the marine perimeter feedback is a driver of self-sustained regrowth and its onset is facilitated by GIA, which reduces the width of marine basins.

By running the retreat branch with atmospheric or oceanic forcing only, we demonstrated that the oceanic contribution dominates at low levels of warming, the atmospheric contribution dominates at high levels of warming and the contributions are mixed in between. This stresses that improving the representation of ice-ocean interactions is paramount to obtain reliable predictions of future sea-level rise, which will take place at levels of warming that are low within the frame of the present work.

The magnitude of AIS hysteresis simulated here is much larger than in previous studies that similarly do not include the melt-albedo feedback (Huybrechts, 1994; Garbe et al., 2020), generally implying committed sea-level rise to be more irreversible than previously assumed. We explained this by the enhanced ocean sensitivity of our setup, which results from two modelling choices supported by recent publications. On one hand, we used a highly non-linear basal friction law, in agreement with laboratory experiments (Zoet and Iverson, 2020). On the other hand, the newly introduced tidal partial melt parametrisation allowed applying melt over the whole grounding zone, as recently measured via synthetic aperture radar (Chen et al., 2023; Rignot et al., 2024). By comparing various simulations, we suggest that ocean sensitivity is an important control on the hysteresis width, while atmospheric sensitivity largely influences the slope of the hysteresis. The large hysteresis obtained here points out that mitigating future sea-level rise is of key importance, since adapting to it might result much more complicated due to the lack of reversibility.

Finally, the bifurcation point of the WAIS obtained in the present study will likely be overshot within the current century, implying a committed sea-level rise of about $4\,\mathrm{mSLE}$ that would be practically irreversible, especially because a subsequent atmospheric cooling might further reduce the AIS volume due to decreased accumulation. In addition, the first bifurcation point of the WSB shows that, under high-emission scenarios, the committed and largely irreversible AIS contribution to sea-level

https://doi.org/10.5194/egusphere-2025-6566
Preprint. Discussion started: 11 February 2026

rise could reach as much as $18\,\mathrm{mSLE}$ and initiate a phase of higher AIS sensitivity to global warming. This further supports that ocean warming and the associated AIS sensitivity are the key controls of future sea-level rise (Coulon et al., 2024, 2025; Fricker et al., 2025), which can only be better constrained by running high-resolution simulations that can simulate ice-ocean interactions over large prediction horizons. In the absence of such a setup, the present study highlights mechanistic explanations of the processes underlying the AIS hysteresis, which can help to better understand future simulations presenting a higher degree of complexity.

Code and data availability. The source code of Yelmo and FastIsostasy can be found at https://github.com/palma-ice/yelmo and https://github.com/palma-ice/FastIsostasy, respectively. They are coupled via Yelmox, which can be found at https://github.com/palma-ice/yelmox. The code used to generate the figures can be found at https://github.com/JanJereczek/rtip-ais. A reduced dataset of the simulation results will be archived upon publication. Due to the sheer size of the full dataset, specific outputs can be shared upon request.

Video supplement. The videos listed in Tab. 1 can be found at:
https://drive.google.com/drive/folders/1W-ZK7PSYJwAxL00RlqqAsOUDMEwAQLbO?usp=sharing

Appendix A: Simulation setup

The work of Garbe et al. (2020) is the most recent study of the AIS hysteresis that presents a similar setup to ours. As mentioned in Sec. 2 and Sec. 4 of the main text, the setups differ mainly through two important modelling choices: the basal friction law and the melting applied at the grounding line, illustrated in Figure A1.

To initialise our simulations, basal friction is optimised during $6\,\mathrm{kyr}$ and then held constant during $4\,\mathrm{kyr}$ such that the final state of the spin-up represents an AIS that is in equilibrium with the present-day climatology. This simulation setup satisfactorily matches the ice surface elevation and velocity, while showing close agreement with the measured grounding-zone position (Fig. A2).

Appendix B: A high-resolution run of the total GIA response to Antarctic deglaciation

Unlike global GIA models, FastIsostasy is capable of simulating the regional GIA response to Antarctic deglaciation at high resolution ($\Delta x = \Delta y = 4\,\mathrm{km}$) in only a few minutes of computation. To this end, the bedrock elevation and ice thickness of BedMachine v3 (Morlighem et al., 2020) for initialisation. The ice thickness is set to 0 for $t > 0$ and the model runs forward in time until $t = 50\,\mathrm{kyr}$, where the bedrock response has converged to equilibrium. The vertical bedrock displacement is interpolated back to the $500\,\mathrm{m}$ grid of BedMachine v3, showing a detailed picture of how the total uplift reduces the extent of marine regions, leads to the emergence of many islands, and decreases the overall retrograde character of the Antarctic bed. These results are very similar to the simulations of Paxman et al. (2022), who obtain a slightly larger uplift due to the

https://doi.org/10.5194/egusphere-2025-6566
Preprint. Discussion started: 11 February 2026

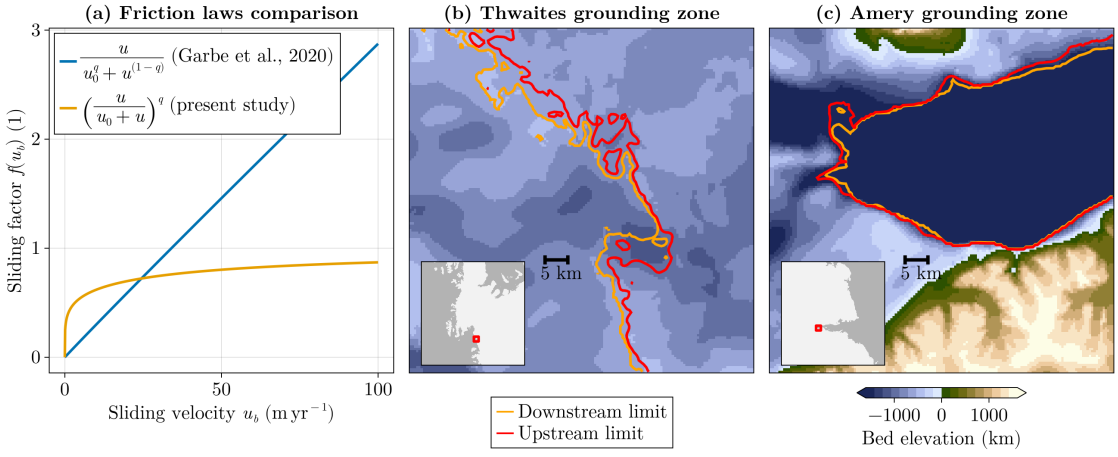

Figure A1. (a) Comparison of the friction coefficient resulting from the power law used in Garbe et al. (2020) and the regularised Coulomb friction law used here. (b-c) When computing the grounding zone limits with PMPT on BedMachine v3, the difference between the downstream and the upstream limit of the grounding zone vary between zero and a few kilometres, which aligns to a large extent with the water infiltrations across the grounding line observed in the Amery and Thwaites regions (Chen et al., 2023; Rignot et al., 2024). In contrast, Garbe et al. (2020) assumes no melt at the grounding line.

inclusion of the still ongoing rebound from LGM. Many of the islands that appear at high resolution are not represented when using $\Delta x = \Delta y = 16$ km, as done in the remainder of this article (Fig. 9). This becomes particularly apparent in regions of high bedrock roughness, as, for instance, in West-Antarctica and the Wilkes basin, where archipelagos arise. This means that significantly increasing the resolution might lead to an easier regrowth of the ice, while limiting the retreat, but this remains to be studied in more detail.

Beside the glaciological implications of newly created archipelagos, we point out that West Antarctica is characterised by low viscosities of the upper mantle, which implies a fast bedrock uplift. This suggests that, if the WAIS collapses over the coming centuries, new islands might emerge before the end of the millennium.

Appendix C: Measuring the relative importance of the perimeter feedback and MISI

To study the relative importance of MISI and the perimeter feedback in the bifurcations of the AIS retreat and regrowth, we define metrics that quantify a necessary condition for their occurrence. In both cases, we require the metric to yield values close to 0 when the process is largely inactive, and to peak to negative (or positive) values when the process is involved in a self-sustained retreat (or readvance). To quantify MISI, we define Φ as:

$$\Phi(\boldsymbol{x}, t) = \mathbb{1}_{\mathrm{mm}} \cdot \max(u_x \cdot \partial_x z_{\mathrm{b}} + u_y \cdot \partial_y z_{\mathrm{b}}, 0) \cdot \partial_t H_{\mathrm{af}}. \tag{C1}$$

https://doi.org/10.5194/egusphere-2025-6566
Preprint. Discussion started: 11 February 2026

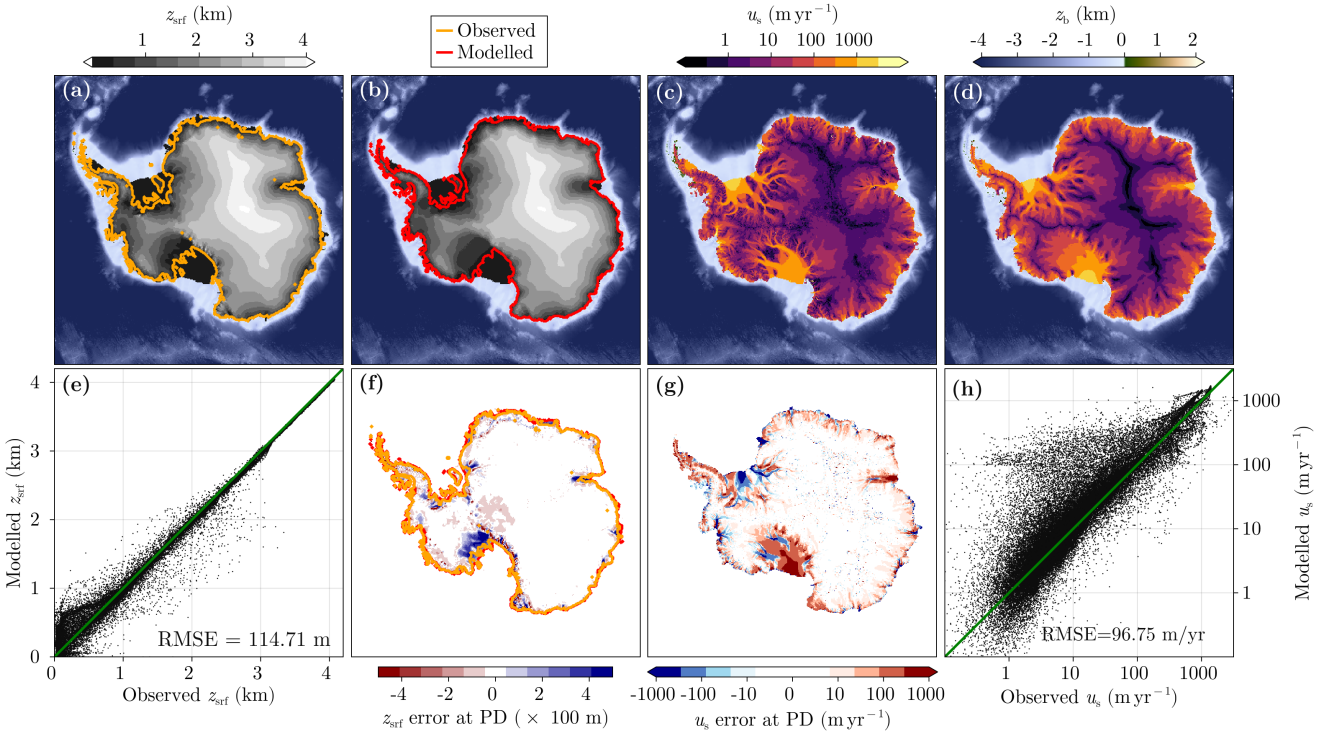

Figure A2. (a) Observed Schaffer et al. (2016) and (b) modelled ice surface elevation at present day. (c) Error plot of the ice surface elevation: the closer to identity (green), the better the fit (black dots). (d) Corresponding error map of surface elevation. a) Observed Rignot et al. (2011) and (b) modelled ice surface velocity at present day. (c) Error plot of the ice surface velocity: the closer to identity (green), the better the fit (black dots). (d) Corresponding error map of surface velocity.

The marine margin is represented by $\mathbb{1}_{\mathrm{mm}}$, an indicator function that yields 1 for a grounding zone below sea level and 0 otherwise. If the bedrock is retrograde, the ice flow at the surface, (u_x, u_y), and the bedrock gradient, $(\partial_x z_\mathrm{b}, \partial_y z_\mathrm{b})$, are aligned, thus yielding a positive scalar product. The second term of Φ excludes negative values of this product, since MISI cannot take place if the bedrock is prograde with respect to ice flow. Finally, MISI is defined by large rates of ice ungrounding at retreat and of ice grounding at regrowth, which is represented by the third term of Φ, responsible for its sign. In summary, this means that Φ yields large absolute values when large rates of ice thickness above flotation are simulated at a marine grounding zone where the flow is aligned with a retrograde bedrock. To conveniently analyse the evolution of Φ in time, we define $\varphi(t) = \min_{\boldsymbol{x}} \Phi(\boldsymbol{x}, t)$ for the retreat and $\varphi(t) = \max_{\boldsymbol{x}} \Phi(\boldsymbol{x}, t)$ for the regrowth. To allow a visualisation with respect to the bifurcation diagram, we plot $\varphi(t)$ against $f(t)$ (Fig. C1.c) and observe, as expected, negative peaks during the MISI-driven collapses (among others, those highlighted in Fig. 3). In contrast, we observe positive peaks during the self-sustained regrowth of marine regions (Fig. C1.d).

https://doi.org/10.5194/egusphere-2025-6566
Preprint. Discussion started: 11 February 2026

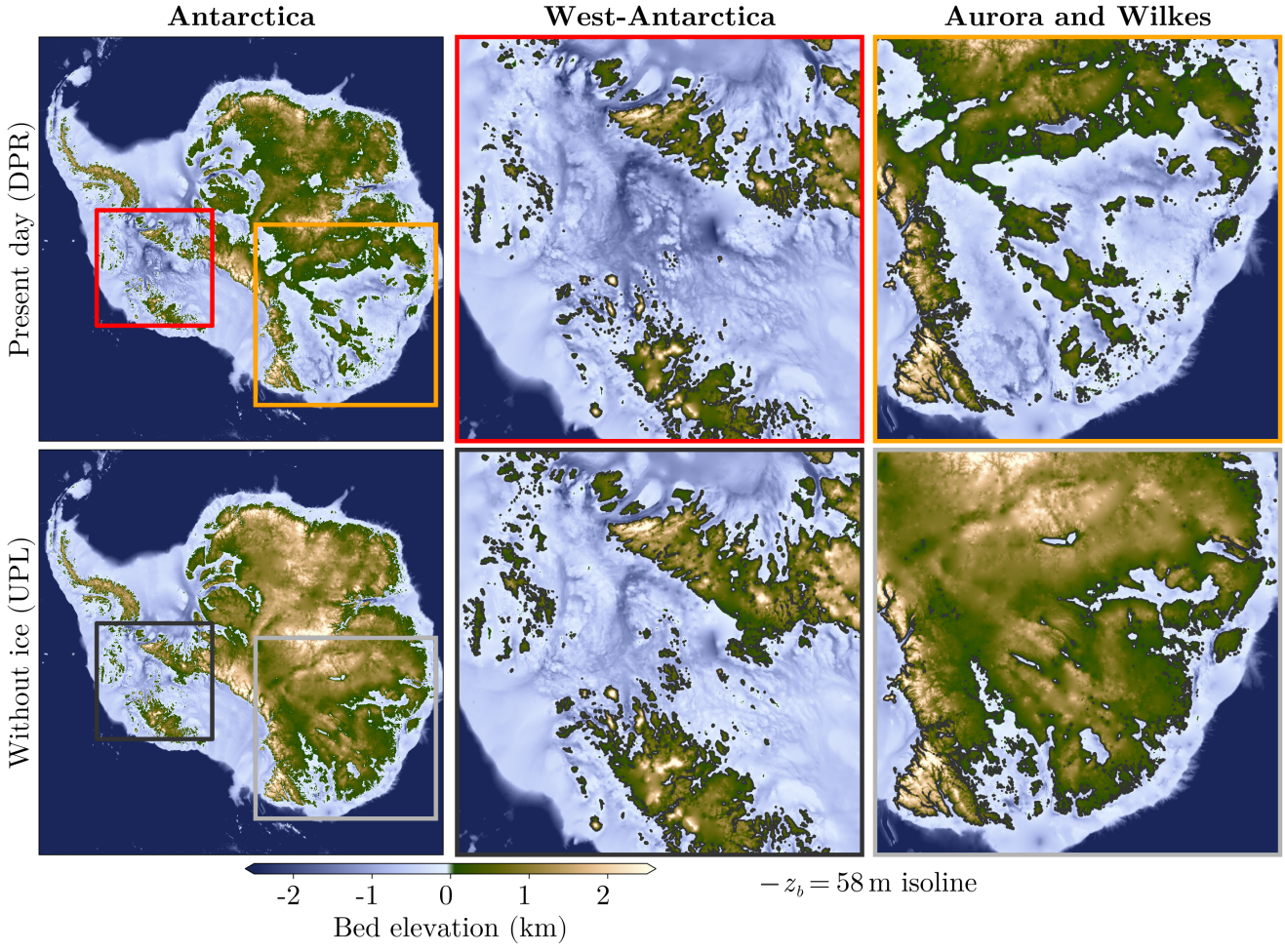

Figure B1. Bathymetry of Antarctica at 500 m resolution; (top) in equilibrium with present-day ice thickness (BedMachine v3); (bottom) in equilibrium with an ice-free continent. The 58 mSLE isoline corresponds to the total AIS volume above flotation.

Furthermore, we define $\Psi(t)$ as the ratio between surface and perimeter, which can be approximated by the ratio between the number of cells that are covered by ice and the number of cells covered by the grounding line. When the perimeter feedback becomes active, Ψ experiences a large decrease at retreat and a large increase at regrowth. Therefore, we define $\psi(t) = \dot{\Psi}(t)$, which, as expected, yields values close to zero when the perimeter feedback is inactive, and large signed values when it becomes active (Fig. C1). During the retreat, all MISI-driven events lead to a more irregular shape of the ice sheet, leading to negative peaks of ψ. As expected for the case of a saddle collapse, the two last self-sustained retreats coincide with peaks of ψ while $\varphi = 0$. The regrowth is marked by positive peaks of ψ (while $\varphi = 0$) that coincide with the mergers of ice caps. At lower temperature anomalies, peaks of ψ coincide with peaks of φ, showing that both mechanisms are active. However, since φ displays larger peaks during the retreat while ψ during regrowth, the relative importance of MISI as a driver of bifurcations

https://doi.org/10.5194/egusphere-2025-6566
Preprint. Discussion started: 11 February 2026

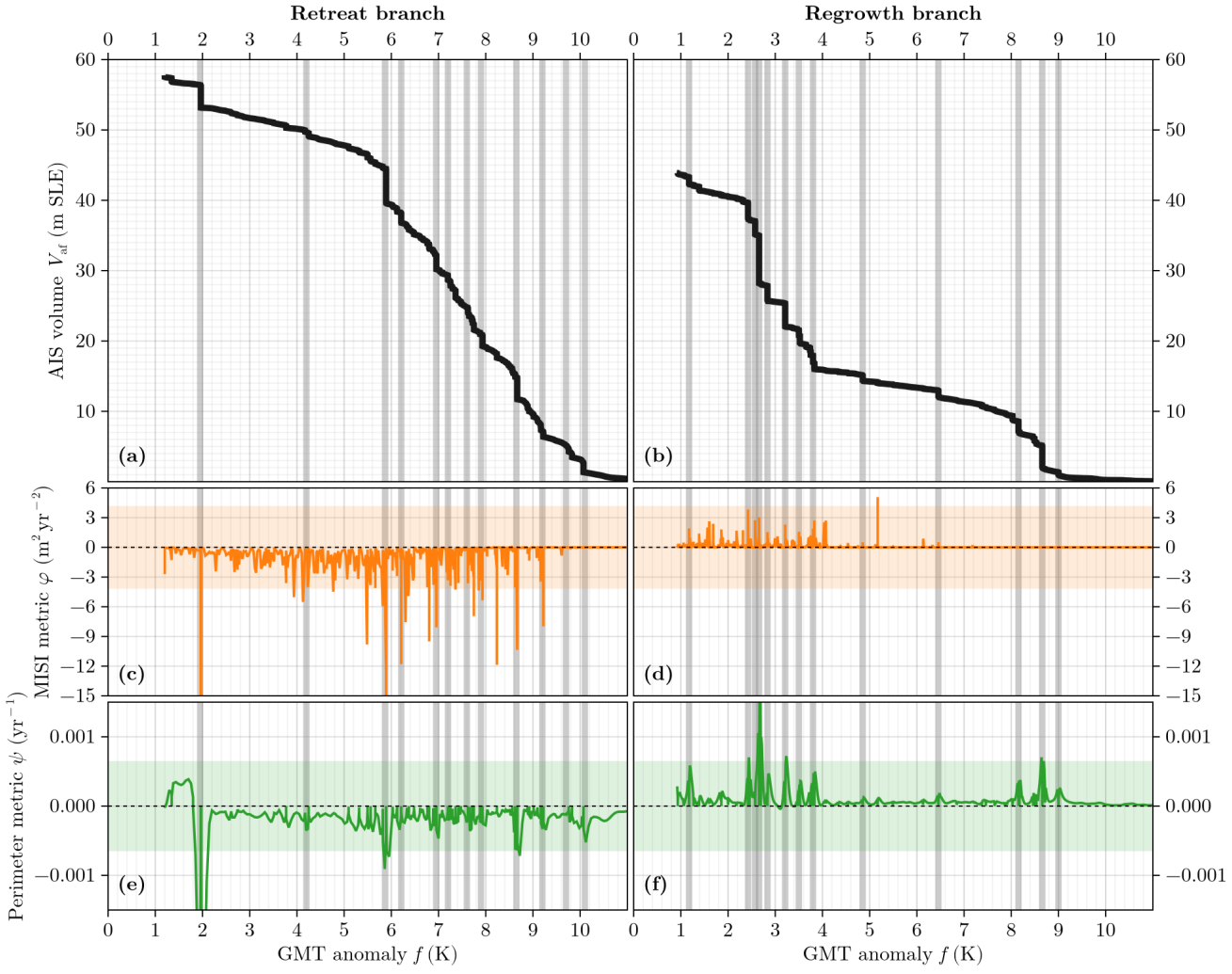

Figure C1. (Equilibrium AIS volume during (a) retreat and (b) regrowth. Corresponding evolution of the (c-d) MISI and (e-f) perimeter metrics. The 3σ-range of each metric is represented by the horizontal shadings, while the vertical shadings highlighted the most important bifurcations, as done in Figures 1 and 4.

is larger during retreat, while the relative importance of the perimeter feedback is larger during regrowth. This is largely due to (1) the reduction of the retrograde bed character due to isostatic uplift (Fig. 9 and Fig. B1), and (2) the more irregular shape of the ice sheet at regrowth (Fig. 5), which is conditioned by the rough coastlines and leads to a high potential of perimeter-driven advances.

We stress that φ and ψ cannot be directly compared against each other, among others, due to their different units. However, as done here, comparing them individually can reveal their relative importance. Furthermore, recognising the process that leads

https://doi.org/10.5194/egusphere-2025-6566
Preprint. Discussion started: 11 February 2026

in time can be very informative to understand which one drives the onset of an instability and which reinforces it. However, the 2D simulation output is sparse due to memory reasons, which prevents detailing this analysis.

Appendix D: Additional examples of perimeter-driven bifurcations

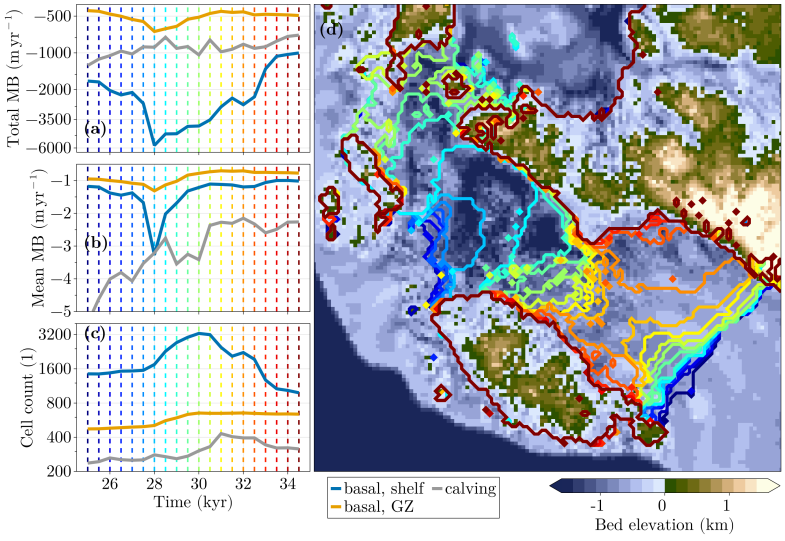

Figure D1. Same as Fig. 8 but illustrating the marine perimeter feedback during the WAIS collapse.

As highlighted throughout the manuscript, the perimeter feedback plays a key role in the AIS hysteresis and multistability. To support this statement, Fig. D1-D4 provide illustrations of this in the case of the WAIS collapse, the ASB collapse, the saddle collapse between the Gamburtsev and Transantarctic Mountains and the abrupt regrowth of the RSB, respectively.

As shown in Fig. C1, the perimeter feedback becomes significantly active during the self-sustained retreat of the WAIS, initiated by MISI around $f = 2\,\mathrm{K}$. This starts with the rapid grounding-zone retreat of Thwaites Glacier, which takes place on a retrograde bedrock and leads to a threefold increase of the total BMB over shelves, driven by a peak in mean BMB ($t = 28\,\mathrm{kyr}$, Fig. D1.a-b). A similar behaviour, albeit with smaller magnitude, is observed for the BMB at the grounding line. After this ($28 < t < 31.5\,\mathrm{kyr}$), the retreat takes place slower, often on a prograde bedrock, and is driven by a total BMB that is still very large, although the mean BMB, both at the grounding zone and over ice shelves, is reduced to values that are smaller than prior to the onset of the collapse. This is explained by the large increase in grounding-zone perimeter and ice-shelf surface area, which both almost experience a doubling (Fig D1.c), with the latter going back to smaller values ($30 < t < 31.5\,\mathrm{kyr}$) due to the melt of large portions of the ice shelves via ocean forcing. At $t = 32\,\mathrm{kyr}$ the saddle covering Siple Coast collapses and leads to a peak in shelf extent and therefore in the associated total BMB (Fig. D1.a-c), leading to a faster retreat again, until the WAIS only covers largely emerged land. This points that a retrograde bedrock is not required throughout the region for the retreat to be self-sustained, due to the perimeter feedback, which is triggered by MISI and reinforces the amplitude of the collapse.

https://doi.org/10.5194/egusphere-2025-6566
Preprint. Discussion started: 11 February 2026

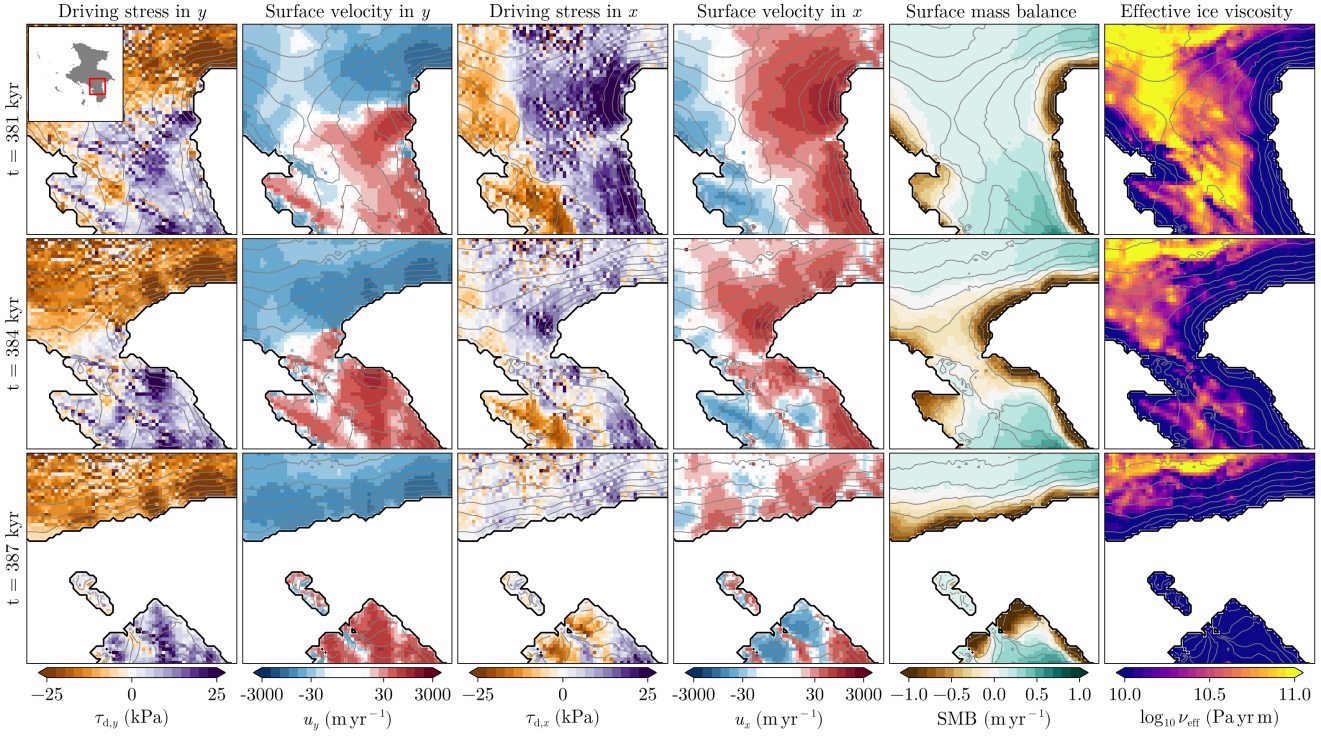

Figure D2. Same as Fig. 6 but illustrating the perimeter feedback during the ASB saddle collapse, shown in Fig. 1.k-l. The normal and tangential directions largely align along y (vertical) and x (horizontal), respectively.

A similar interplay of the mechanisms can also take place for a continental saddle collapse: the MISI-driven retreat of the ASB (Fig. 2.g-h, Fig. 3 bottom line), leads to a very irregular shape of the margin, leading to a large negative SMB and tangential ice flow (aligned with x, Fig. D2, $t = 381\,\text{kyr}$). This drives the saddle collapse (Fig. D2, $t = 384\,\text{kyr}$), marked by larger regions of negative SMB, reduced ice viscosity and a reorientation of the flow towards the normal direction (aligned with y, Fig. D2, $t = 387\,\text{kyr}$). This points out that, even in the absence of the melt-albedo feedback, the MISI-driven collapse of EASBs can have a significant impact on the EAIS interior via a cascade of positive feedbacks. The EAIS interior itself is subject to purely continental saddle collapses, as illustrated in Fig. D3.

As in the case of the ASB, the abrupt RSB regrowth simulated at $f = 3.1\,\text{K}$ begins with the advance of the grounding zone over an island (Fig. D4, $t = 504\,\text{kyr}$), this reduces the perimeter of the grounding and the associated total BMB, leading to a self-sustained advance although the mean BMB remains constant. By the same geometrical effect, the overall calving is decreased. Contrary to the case of the ASB, the number of ice-shelf cells increases over this event but remains very low, thus being of reduced importance compared to the grounding-zone BMB.

https://doi.org/10.5194/egusphere-2025-6566
Preprint. Discussion started: 11 February 2026

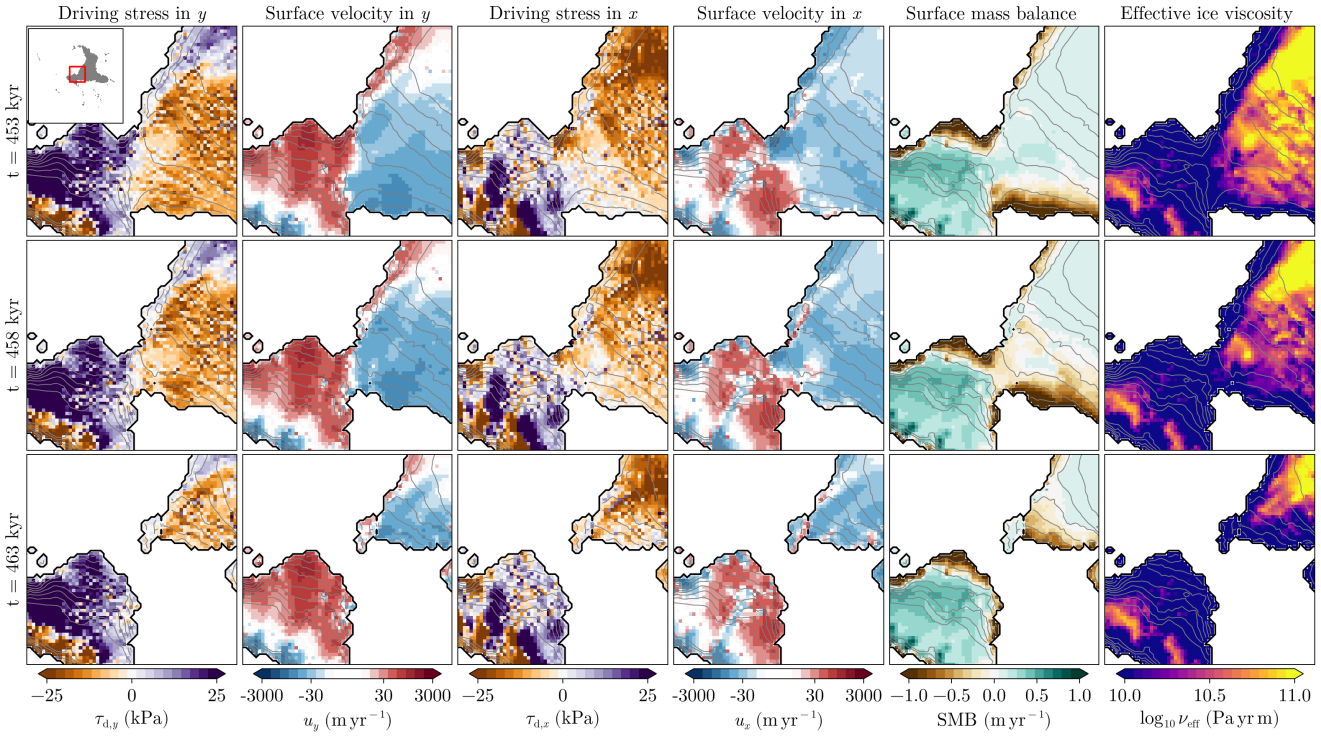

Figure D3. Same as Fig. 6 but illustrating the perimeter feedback during the saddle collapse between the Gamburtsev and the Transantarctic Mountains.

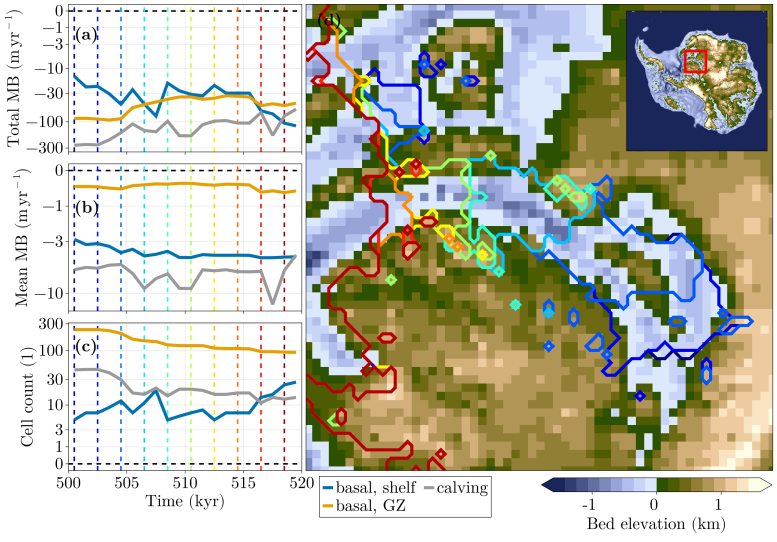

Figure D4. Same as Fig. 8 but illustrating the marine perimeter feedback during the abrupt regrowth of the RSB.

https://doi.org/10.5194/egusphere-2025-6566
Preprint. Discussion started: 11 February 2026

Author contributions. J.S-J., J.A-S., A.R. and M.M. conceptually designed the present study. J.S-J., J.A-S. and A.R. performed the model calibration. J.S-J. ran the simulations and redacted the manuscript with contributions from all co-authors.

Competing interests. A.R. is a member of the editorial board of The Cryosphere.

Acknowledgements. J.S-J. would like to thank the Potsdam Institute for Climate Impact Research, in particular Matteo Willeit and Andrey Ganopolski, for the provided computational resources.

Funding. Jan Swierczek-Jereczek received funding from the EU H2020 research infrastructures of the European Commission (CriticalEarth, grant no. 956170 & ClimTip, grant no. 101137601). Marisa Montoya and Jorge Alvarez-Solas received funding from the Spanish Ministry of Science, Innovation and Universities (project CREEP & project CCRYTICAS, grant no. PID2022-142800OB-I00). Alexander Robinson received funding from the European Research Council (ERC Consolidator grant, FORCLIMA, grant no. 101044247). Lucía Gutierrez-Gonzalez received funding from the autonomous Community of Madrid (grant no. PIPF-2023/COM-30410).

https://doi.org/10.5194/egusphere-2025-6566
Preprint. Discussion started: 11 February 2026

References

Albrecht, T., Bagge, M., and Klemann, V.: Feedback mechanisms controlling Antarctic glacial-cycle dynamics simulated with a coupled ice sheet–solid Earth model, The Cryosphere, 18, 4233–4255, https://doi.org/10.5194/tc-18-4233-2024, 2024.

Armstrong McKay, D. I., Staal, A., Abrams, J. F., Winkelmann, R., Sakschewski, B., Loriani, S., Fetzer, I., Cornell, S. E., Rockström, J., and Lenton, T. M.: Exceeding 1.5°C global warming could trigger multiple climate tipping points, Science, 377, eabn7950, https://doi.org/10.1126/science.abn7950, 2022.

Bastiaansen, R., Dijkstra, H. A., and von der Heydt, A. S.: Fragmented tipping in a spatially heterogeneous world, Environmental Research Letters, 17, 045 006, https://doi.org/10.1088/1748-9326/ac59a8, 2022.

Bintanja, R. and Van De Wal, R. S. W.: North American ice-sheet dynamics and the onset of 100,000-year glacial cycles, Nature, 454, 869–872, https://doi.org/10.1038/nature07158, 2008.

Bochow, N., Poltronieri, A., Robinson, A., Montoya, M., Rypdal, M., and Boers, N.: Overshooting the critical threshold for the Greenland ice sheet, Nature, 622, 528–536, https://doi.org/10.1038/s41586-023-06503-9, 2023.

Bueler, E. and van Pelt, W.: Mass-conserving subglacial hydrology in the Parallel Ice Sheet Model version 0.6, Geosci. Model Dev., https://doi.org/https://doi.org/10.5194/gmd-8-1613-2015, 2015.

Chen, H., Rignot, E., Scheuchl, B., and Ehrenfeucht, S.: Grounding Zone of Amery Ice Shelf, Antarctica, From Differential Synthetic-Aperture Radar Interferometry, Geophysical Research Letters, 50, e2022GL102 430, https://doi.org/10.1029/2022GL102430, 2023.

Christianson, K., Jacobel, R. W., Horgan, H. J., Alley, R. B., Anandakrishnan, S., Holland, D. M., and DallaSanta, K. J.: Basal conditions at the grounding zone of Whillans Ice Stream, West Antarctica, from ice-penetrating radar, Journal of Geophysical Research: Earth Surface, 121, 1954–1983, https://doi.org/10.1002/2015JF003806, 2016.

Clarke, G. K. C., Nitsan, U., and Paterson, W. S. B.: Strain heating and creep instability in glaciers and ice sheets, Reviews of Geophysics, 15, 235–247, https://doi.org/10.1029/RG015i002p00235, 1977.

Coulon, V., Klose, A. K., Kittel, C., Edwards, T., Turner, F., Winkelmann, R., and Pattyn, F.: Disentangling the drivers of future Antarctic ice loss with a historically calibrated ice-sheet model, The Cryosphere, 18, 653–681, https://doi.org/10.5194/tc-18-653-2024, 2024.

Coulon, V., Klose, A. K., Edwards, T., Turner, F., Pattyn, F., and Winkelmann, R.: From short-term uncertainties to long-term certainties in the future evolution of the Antarctic Ice Sheet, Nature Communications, 16, 10 385, https://doi.org/10.1038/s41467-025-66178-w, publisher: Nature Publishing Group, 2025.

Favier, L., Jourdain, N. C., Jenkins, A., Merino, N., Durand, G., Gagliardini, O., Gillet-Chaulet, F., and Mathiot, P.: Assessment of sub-shelf melting parameterisations using the ocean–ice-sheet coupled model NEMO(v3.6)–Elmer/Ice(v8.3), Geoscientific Model Development, 12, 2255–2283, https://doi.org/10.5194/gmd-12-2255-2019, 2019.

Fox-Kemper, B., Hewitt, H. T., Xiao, C., Aðalgeirsdóttir, G., Drijfhout, S. S., Edwards, T. L., Golledge, N. R., Hemer, M., Kopp, R. E., Krinner, G., Mix, A., Notz, D., Nowicki, S., Nurhati, I. S., Ruiz, L., Sallée, J.-B., Slangen, A. B. A., Stammer, D., Timmermann, A., Timm, O., van de Wal, R. S. W., and van den Broeke, M.: Chapter 9: Ocean, Cryosphere and Sea Level Change, in: Climate Change 2021: The Physical Science Basis. Contribution of Working Group I to the Sixth Assessment Report of the Intergovernmental Panel on Climate Change, edited by Masson-Delmotte, V., Zhai, P., Pirani, A., Connors, S. L., Péan, C., Berger, S., Caud, N., Chen, Y., Goldfarb, L., Gomis, M. I., Huang, M., Leitzell, K., Lonnoy, E., Matthews, J. B. R., Maycock, T. K., Waterfield, T., Yelekçi, O., Yu, R., and Zhou, B., Cambridge University Press, Cambridge, United Kingdom and New York, NY, USA, https://doi.org/10.1017/9781009157896.011, 2021.

https://doi.org/10.5194/egusphere-2025-6566
Preprint. Discussion started: 11 February 2026

Fricker, H. A., Galton-Fenzi, B. K., Walker, C. C., Freer, B. I. D., Padman, L., and DeConto, R.: Antarctica in 2025: Drivers of deep uncertainty in projected ice loss, Science, 387, 601–609, https://doi.org/10.1126/science.adt9619, 2025.

Garbe, J., Albrecht, T., Levermann, A., Donges, J., and Winkelmann, R.: The hysteresis of the Antarctic Ice Sheet, Nature, 585, 538–544, https://doi.org/10.1038/s41586-020-2727-5, 2020.

Gauthier, M. S., Kelley, S. E., and Hodder, T. J.: Lake Agassiz drainage bracketed Holocene Hudson Bay Ice Saddle collapse, Earth and Planetary Science Letters, 544, 116 372, https://doi.org/10.1016/j.epsl.2020.116372, 2020.

Goelzer, H., Coulon, V., Pattyn, F., de Boer, B., and van de Wal, R.: Brief communication: On calculating the sea-level contribution in marine ice-sheet models, The Cryosphere, 14, 833–840, https://doi.org/10.5194/tc-14-833-2020, 2020.

Goldberg, D. N.: A variationally derived, depth-integrated approximation to a higher-order glaciological flow model, Journal of Glaciology, 57, 157–170, https://doi.org/10.3189/002214311795306763, 2011.

Golledge, N. R., Kowalewski, D. E., Naish, T. R., Levy, R. H., Fogwill, C. J., and Gasson, E. G. W.: The multi-millennial Antarctic commitment to future sea-level rise, Nature, 526, 421–425, https://doi.org/10.1038/nature15706, 2015.

Gomez, N., Pollard, D., Mitrovica, J. X., Huybers, P., and Clark, P. U.: Evolution of a coupled marine ice sheet-sea level model, Journal of Geophysical Research: Earth Surface, 117, https://doi.org/10.1029/2011JF002128, 2012.

Gomez, N., Gregoire, L. J., Mitrovica, J. X., and Payne, A. J.: Laurentide-Cordilleran Ice Sheet saddle collapse as a contribution to meltwater pulse 1A, Geophysical Research Letters, 42, 3954–3962, https://doi.org/10.1002/2015GL063960, 2015.

Gomez, N., Yousefi, M., Pollard, D., DeConto, R. M., Sadai, S., Lloyd, A., Nyblade, A., Wiens, D. A., Aster, R. C., and Wilson, T.: The influence of realistic 3D mantle viscosity on Antarctica's contribution to future global sea levels, Science Advances, 10, eadn1470, https://doi.org/10.1126/sciadv.adn1470, 2024.

Gregoire, L. J., Payne, A. J., and Valdes, P. J.: Deglacial rapid sea level rises caused by ice-sheet saddle collapses, Nature, 487, 219–222, https://doi.org/10.1038/nature11257, 2012.

Gregoire, L. J., Otto-Bliesner, B., Valdes, P. J., and Ivanovic, R.: Abrupt Bølling warming and ice saddle collapse contributions to the Meltwater Pulse 1a rapid sea level rise, Geophysical Research Letters, 43, 9130–9137, https://doi.org/10.1002/2016GL070356, 2016.

Hansen, J., Sato, M., Russell, G., and Kharecha, P.: Climate sensitivity, sea level and atmospheric carbon dioxide, Philosophical Transactions of the Royal Society A: Mathematical, Physical and Engineering Sciences, 371, 20120 294, https://doi.org/10.1098/rsta.2012.0294, 2013.

Hazzard, J. A. N. and Richards, F. D.: Antarctic Geothermal Heat Flow, Crustal Conductivity and Heat Production Inferred From Seismological Data, Geophysical Research Letters, 51, e2023GL106 274, https://doi.org/10.1029/2023GL106274, 2024.

Huybrechts, P.: Formation and disintegration of the Antarctic ice sheet, Annals of Glaciology, 20, 336–340, https://doi.org/10.3189/1994AoG20-1-336-340, 1994.

Ji, W., Robel, A., Tziperman, E., and Yang, J.: Laurentide Ice Saddle Mergers Drive Rapid Sea Level Drops During Glaciations, Geophysical Research Letters, 48, e2021GL094 263, https://doi.org/10.1029/2021GL094263, _eprint: https://agupubs.onlinelibrary.wiley.com/doi/pdf/10.1029/2021GL094263, 2021.

Jourdain, N. C., Asay-Davis, X., Hattermann, T., Straneo, F., Seroussi, H., Little, C. M., and Nowicki, S.: A protocol for calculating basal melt rates in the ISMIP6 Antarctic ice sheet projections, The Cryosphere, 14, 3111–3134, https://doi.org/10.5194/tc-14-3111-2020, 2020.

Klose, A. K., Coulon, V., Pattyn, F., and Winkelmann, R.: The long-term sea-level commitment from Antarctica, The Cryosphere, 18, 4463–4492, https://doi.org/10.5194/tc-18-4463-2024, 2024.

Kulp, S. A. and Strauss, B. H.: New elevation data triple estimates of global vulnerability to sea-level rise and coastal flooding, Nature Communications, 10, 4844, https://doi.org/10.1038/s41467-019-12808-z, 2019.

https://doi.org/10.5194/egusphere-2025-6566
Preprint. Discussion started: 11 February 2026

Leguy, G. R., Lipscomb, W. H., and Asay-Davis, X. S.: Marine ice sheet experiments with the Community Ice Sheet Model, The Cryosphere, 15, 3229–3253, https://doi.org/10.5194/tc-15-3229-2021, 2021.

Leloup, G., Quiquet, A., Roche, D. M., Dumas, C., and Paillard, D.: Hysteresis of the Antarctic Ice Sheet With a Coupled Climate-Ice-Sheet Model, Geophysical Research Letters, 52, https://doi.org/https://doi.org/10.1029/2024GL111492, 2025.

Lipscomb, W. H., Price, S. F., Hoffman, M. J., Leguy, G. R., Bennett, A. R., Bradley, S. L., Evans, K. J., Fyke, J. G., Kennedy, J. H., Perego, M., Ranken, D. M., Sacks, W. J., Salinger, A. G., Vargo, L. J., and Worley, P. H.: Description and evaluation of the Community Ice Sheet Model (CISM) v2.1, Geoscientific Model Development, 12, 387–424, https://doi.org/10.5194/gmd-12-387-2019, 2019.

Lipscomb, W. H., Behar, D., and Morrison, M. A.: Brief communication: Sea-level projections, adaptation planning, and actionable science, The Cryosphere, 19, 793–803, https://doi.org/10.5194/tc-19-793-2025, 2025.

Lochte, A. A., Repschläger, J., Kienast, M., Garbe-Schönberg, D., Andersen, N., Hamann, C., and Schneider, R.: Labrador Sea freshening at 8.5 ka BP caused by Hudson Bay Ice Saddle collapse, Nature Communications, 10, 586, https://doi.org/10.1038/s41467-019-08408-6, publisher: Nature Publishing Group, 2019.

Matero, I. S. O., Gregoire, L. J., Ivanovic, R. F., Tindall, J. C., and Haywood, A. M.: The 8.2 ka cooling event caused by Laurentide ice saddle collapse, Earth and Planetary Science Letters, 473, 205–214, https://doi.org/10.1016/j.epsl.2017.06.011, 2017.

Matero, I. S. O., Gregoire, L. J., and Ivanovic, R. F.: Simulating the Early Holocene demise of the Laurentide Ice Sheet with BISICLES (public trunk revision 3298), Geoscientific Model Development, 13, 4555–4577, https://doi.org/10.5194/gmd-13-4555-2020, publisher: Copernicus GmbH, 2020.

Miller, K. G., Browning, J. V., Schmelz, W. J., Kopp, R. E., Mountain, G. S., and Wright, J. D.: Cenozoic sea-level and cryospheric evolution from deep-sea geochemical and continental margin records, Science Advances, 6, https://doi.org/10.1126/sciadv.aaz1346, 2020.

Moreno-Parada, D., Robinson, A., Montoya, M., and Alvarez-Solas, J.: Description and validation of the ice-sheet model Nix v1.0, Geoscientific Model Development, 18, 3895–3919, https://doi.org/10.5194/gmd-18-3895-2025, publisher: Copernicus GmbH, 2025.

Morlighem, M., Rignot, E., Binder, T., Blankenship, D., Drews, R., Eagles, G., Eisen, O., Ferraccioli, F., Forsberg, R., Fretwell, P., Goel, V., Greenbaum, J. S., Gudmundsson, H., Guo, J., Helm, V., Hofstede, C., Howat, I., Humbert, A., Jokat, W., Karlsson, N. B., Lee, W. S., Matsuoka, K., Millan, R., Mouginot, J., Paden, J., Pattyn, F., Roberts, J., Rosier, S., Ruppel, A., Seroussi, H., Smith, E. C., Steinhage, D., Sun, B., Broeke, M. R. V. D., Ommen, T. D. V., Wessem, M. V., and Young, D. A.: Deep glacial troughs and stabilizing ridges unveiled beneath the margins of the Antarctic ice sheet, Nature Geoscience, 13, 132–137, https://doi.org/10.1038/s41561-019-0510-8, 2020.

Morlighem, M., Goldberg, D., Barnes, J. M., Bassis, J. N., Benn, D. I., Crawford, A. J., Gudmundsson, G. H., and Seroussi, H.: The West Antarctic Ice Sheet may not be vulnerable to marine ice cliff instability during the 21st century, Science Advances, 10, eado7794, https://doi.org/10.1126/sciadv.ado7794, 2024.

Paxman, G. J. G., Austermann, J., and Hollyday, A.: Total isostatic response to the complete unloading of the Greenland and Antarctic Ice Sheets, Scientific Reports, 12, 11 399, https://doi.org/10.1038/s41598-022-15440-y, 2022.

Payne, A. and Sugden, D.: Topography and ice sheet growth, Earth Surface Processes and Landforms, 15, 625–639, https://doi.org/10.1002/esp.3290150705, 1990.

Pollard, D. and DeConto, R. M.: Hysteresis in Cenozoic Antarctic ice-sheet variations, Global and Planetary Change, 45, 9–21, https://doi.org/10.1016/j.gloplacha.2004.09.011, 2005.

Pollard, D., DeConto, R. M., and Alley, R. B.: Potential Antarctic Ice Sheet retreat driven by hydrofracturing and ice cliff failure, Earth and Planetary Science Letters, 412, 112–121, https://doi.org/10.1016/j.epsl.2014.12.035, 2015.

https://doi.org/10.5194/egusphere-2025-6566
Preprint. Discussion started: 11 February 2026

Reeh, N.: Dynamic and Climatic History of the Greenland Ice Sheet, in: Quaternary Geology of Canada and Greenland, Geological Society of America, geological society of america edn., ISBN 978-0-8137-5460-4, 1989.

Reyes, A. V., Carlson, A. E., Clark, J., Guillaume, L., Milne, G. A., Tarasov, L., Carlson, E. C. B., He, F., Caffee, M. W., Wilcken, K. M., and Rood, D. H.: Timing of Cordilleran-Laurentide ice-sheet separation: Implications for sea-level rise, Quaternary Science Reviews, 328, 108 554, https://doi.org/10.1016/j.quascirev.2024.108554, 2024.

Riahi, K., van Vuuren, D. P., Kriegler, E., Edmonds, J., O'Neill, B. C., Fujimori, S., Bauer, N., Calvin, K., Dellink, R., Fricko, O., Lutz, W., Popp, A., Cuaresma, J. C., Kc, S., Leimbach, M., Jiang, L., Kram, T., Rao, S., Emmerling, J., Ebi, K., Hasegawa, T., Havlik, P., Humpenöder, F., Da Silva, L. A., Smith, S., Stehfest, E., Bosetti, V., Eom, J., Gernaat, D., Masui, T., Rogelj, J., Strefler, J., Drouet, L., Krey, V., Luderer, G., Harmsen, M., Takahashi, K., Baumstark, L., Doelman, J. C., Kainuma, M., Klimont, Z., Marangoni, G., Lotze-Campen, H., Obersteiner, M., Tabeau, A., and Tavoni, M.: The Shared Socioeconomic Pathways and their energy, land use, and greenhouse gas emissions implications: An overview, Global Environmental Change, 42, 153–168, https://doi.org/10.1016/j.gloenvcha.2016.05.009, 2017.

Rignot, E., Mouginot, J., and Scheuchl, B.: Ice Flow of the Antarctic Ice Sheet, Science, 333, 1427–1430, https://doi.org/10.1126/science.1208336, 2011.

Rignot, E., Ciracì, E., Scheuchl, B., Tolpekin, V., Wollersheim, M., and Dow, C.: Widespread seawater intrusions beneath the grounded ice of Thwaites Glacier, West Antarctica, Proceedings of the National Academy of Sciences, 121, e2404766 121, https://doi.org/10.1073/pnas.2404766121, 2024.

Robel, A. A., Wilson, E., and Seroussi, H.: Layered seawater intrusion and melt under grounded ice, The Cryosphere, 16, 451–469, https://doi.org/10.5194/tc-16-451-2022, 2022.

Robinson, A., Alvarez-Solas, J., Montoya, M., Goelzer, H., Greve, R., and Ritz, C.: Description and validation of the ice-sheet model Yelmo (version 1.0), Geoscientific Model Development, 13, 2805–2823, https://doi.org/10.5194/gmd-13-2805-2020, 2020.

Robinson, A., Goldberg, D., and Lipscomb, W. H.: A comparison of the stability and performance of depth-integrated ice-dynamics solvers, The Cryosphere, 16, 689–709, https://doi.org/10.5194/tc-16-689-2022, 2022.

Ross, N., Milillo, P., Nakshatrala, K. B., Ballarini, R., Stubblefield, A., and Dini, L.: Importance of ice elasticity in simulating tide-induced grounding line variations along prograde bed slopes, https://doi.org/10.5194/egusphere-2024-875, 2024.

Schaffer, J., Timmermann, R., Arndt, J. E., Kristensen, S. S., Mayer, C., Morlighem, M., and Steinhage, D.: A global, high-resolution data set of ice sheet topography, cavity geometry, and ocean bathymetry, Earth System Science Data, 8, 543–557, https://doi.org/10.5194/essd-8-543-2016, 2016.

Schoof, C.: Ice sheet grounding line dynamics: Steady states, stability, and hysteresis, Journal of Geophysical Research, 112, F03S28, https://doi.org/10.1029/2006JF000664, 2007.

Seroussi, H., Nowicki, S., Payne, A. J., Goelzer, H., Lipscomb, W. H., Abe-Ouchi, A., Agosta, C., Albrecht, T., Asay-Davis, X., Barthel, A., Calov, R., Cullather, R., Dumas, C., Galton-Fenzi, B. K., Gladstone, R., Golledge, N. R., Gregory, J. M., Greve, R., Hattermann, T., Hoffman, M. J., Humbert, A., Huybrechts, P., Jourdain, N. C., Kleiner, T., Larour, E., Leguy, G. R., Lowry, D. P., Little, C. M., Morlighem, M., Pattyn, F., Pelle, T., Price, S. F., Quiquet, A., Reese, R., Schlegel, N.-J., Shepherd, A., Simon, E., Smith, R. S., Straneo, F., Sun, S., Trusel, L. D., Van Breedam, J., Van De Wal, R. S. W., Winkelmann, R., Zhao, C., Zhang, T., and Zwinger, T.: ISMIP6 Antarctica: a multi-model ensemble of the Antarctic ice sheet evolution over the 21st century, The Cryosphere, 14, 3033–3070, https://doi.org/10.5194/tc-14-3033-2020, 2020.

https://doi.org/10.5194/egusphere-2025-6566
Preprint. Discussion started: 11 February 2026

Seroussi, H., Pelle, T., Lipscomb, W. H., Abe-Ouchi, A., Albrecht, T., Alvarez-Solas, J., Asay-Davis, X., Barre, J., Berends, C. J., Bernales, J., Blasco, J., Caillet, J., Chandler, D. M., Coulon, V., Cullather, R., Dumas, C., Galton-Fenzi, B. K., Garbe, J., Gillet-Chaulet, F., Gladstone, R., Goelzer, H., Golledge, N., Greve, R., Gudmundsson, G. H., Han, H. K., Hillebrand, T. R., Hoffman, M. J., Huybrechts, P., Jourdain, N. C., Klose, A. K., Langebroek, P. M., Leguy, G. R., Lowry, D. P., Mathiot, P., Montoya, M., Morlighem, M., Nowicki, S., Pattyn, F., Payne, A. J., Quiquet, A., Reese, R., Robinson, A., Saraste, L., Simon, E. G., Sun, S., Twarog, J. P., Trusel, L. D., Urruty, B., Van Breedam, J., Van De Wal, R. S. W., Wang, Y., Zhao, C., and Zwinger, T.: Evolution of the Antarctic Ice Sheet Over the Next Three Centuries From an ISMIP6 Model Ensemble, Earth's Future, 12, e2024EF004 561, https://doi.org/10.1029/2024EF004561, 2024.

Smith, D. M., Screen, J. A., Deser, C., Cohen, J., Fyfe, J. C., García-Serrano, J., Jung, T., Kattsov, V., Matei, D., Msadek, R., Peings, Y., Sigmond, M., Ukita, J., Yoon, J.-H., and Zhang, X.: The Polar Amplification Model Intercomparison Project (PAMIP) contribution to CMIP6: investigating the causes and consequences of polar amplification, Geoscientific Model Development, 12, 1139–1164, https://doi.org/10.5194/gmd-12-1139-2019, 2019.

Swierczek-Jereczek, J., Montoya, M., Latychev, K., Robinson, A., Alvarez-Solas, J., and Mitrovica, J.: FastIsostasy v1.0 – a regional, accelerated 2D glacial isostatic adjustment (GIA) model accounting for the lateral variability of the solid Earth, Geoscientific Model Development, 17, 5263–5290, https://doi.org/10.5194/gmd-17-5263-2024, 2024.

The IMBIE team: Mass balance of the Antarctic Ice Sheet from 1992 to 2017, Nature, 558, 219–222, https://doi.org/10.1038/s41586-018-0179-y, 2018.

Van Breedam, J., Huybrechts, P., and Crucifix, M.: Hysteresis and orbital pacing of the early Cenozoic Antarctic ice sheet, Climate of the Past, 19, 2551–2568, https://doi.org/10.5194/cp-19-2551-2023, 2023.

Van Den Akker, T., Lipscomb, W. H., Leguy, G. R., Bernales, J., Berends, C. J., Van De Berg, W. J., and Van De Wal, R. S. W.: Present-day mass loss rates are a precursor for West Antarctic Ice Sheet collapse, The Cryosphere, 19, 283–301, https://doi.org/10.5194/tc-19-283-2025, 2025.

Van Wessem, J. M., Van De Berg, W. J., and Van Den Broeke, M. R.: Data Set: Monthly Averaged RACMO2.3p2 Variables; Antarctica, https://doi.org/https://dx.doi.org/10.5281/zenodo.7760491, 2023.

Weertman, J.: Stability of the Junction of an Ice Sheet and an Ice Shelf, Journal of Glaciology, 13, 3–11, https://doi.org/10.3189/S0022143000023327, 1974.

Westerhold, T., Marwan, N., Drury, A. J., Liebrand, D., Agnini, C., Anagnostou, E., Barnet, J. S. K., Bohaty, S. M., De Vleeschouwer, D., Florindo, F., Frederichs, T., Hodell, D. A., Holbourn, A. E., Kroon, D., Lauretano, V., Littler, K., Lourens, L. J., Lyle, M., Pälike, H., Röhl, U., Tian, J., Wilkens, R. H., Wilson, P. A., and Zachos, J. C.: An astronomically dated record of Earth's climate and its predictability over the last 66 million years, Science, 369, 1383–1387, https://doi.org/10.1126/science.aba6853, 2020.

Whitehouse, P. L., Gomez, N., King, M. A., and Wiens, D. A.: Solid Earth change and the evolution of the Antarctic Ice Sheet, Nature Communications, 10, 503, https://doi.org/10.1038/s41467-018-08068-y, 2019.

Wirths, C., Hermant, A., Stepanek, C., Stocker, T. F., and Sutter, J. C. R.: Sequence of abrupt transitions in Antarctic drainage basins before and during the Mid-Pleistocene Transition, Nature Communications, 16, 10 391, https://doi.org/10.1038/s41467-025-65375-x, publisher: Nature Publishing Group, 2025.

Zoet, L. K. and Iverson, N. R.: A slip law for glaciers on deformable beds, Science, 368, 76–78, https://doi.org/10.1126/science.aaz1183, 2020.